Reviews in Mineralogy & Geochemistry
Vol. 86 pp. 429–462, 2021

Triple Oxygen Isotopes in Meteoric Waters, Carbonates, and Biological Apatites: Implications for Continental Paleoclimate Reconstruction

Benjamin H. Passey and Naomi E. Levin

Department of Earth and Environmental Sciences
University of Michigan
1100 North University Avenue
Ann Arbor, MI, 48103
USA

passey@umich.edu

nelevin@umich.edu

INTRODUCTION

The usefulness of triple isotope studies of natural systems is contingent on the existence of resolvable differences in mass-dependent fractionation exponents θ [where $\theta = \ln(^{17}/^{16}\alpha)/\ln(^{18}/^{16}\alpha)$] among processes that are prevalent in the system(s) of interest, or on the existence of resolvable non-mass-dependent fractionation in the system. Both such contingencies are satisfied in continental hydroclimate systems. The process of evaporation of water involves molecular diffusion of water vapor through air, which carries a θ value of 0.5185 (Barkan and Luz 2007) that differs strongly from the value of 0.529 for equilibrium exchange between water vapor and liquid water (Barkan and Luz 2005). This means that waters that have been isotopically modified by evaporation can, in many cases, be clearly identified on the basis of triple oxygen isotope analysis (Landais et al. 2006; Surma et al. 2015, 2018; Gázquez et al. 2018), and that it may even be possible to reconstruct the isotopic composition of the unevaporated source waters (Passey and Ji 2019). Leaf waters are highly evaporated and have distinctive triple oxygen isotope compositions (Landais et al. 2006; Li et al. 2017), which has implications for the triple oxygen isotope compositions of atmospheric CO_2 and O_2 (Liang et al. 2017), plant materials such as cellulose and phytoliths (Alexandre et al. 2018), and animals that ingest significant amounts of leaf water (Pack et al. 2013; Passey et al. 2014).

Molecular oxygen in the atmosphere is strongly fractionated in a non-mass-dependent way due to photochemically-driven isotopic exchange in the stratosphere (Luz et al. 1999; Bao et al. 2008; Pack 2021, this volume), with the degree of fractionation dependent on pCO_2, pO_2, and global gross primary productivity (GPP) (Cao and Bao 2013; Young et al. 2014). Through the process of respiration, this oxygen with $\Delta'^{17}O$ of approximately –430 per meg (Barkan and Luz 2005; Pack et al. 2017; Wostbrock et al. 2020) can become part of body water and hence biominerals (Pack et al. 2013). Note that in this chapter, we calculate $\Delta'^{17}O$ as: $\Delta'^{17}O = \delta'^{17}O - 0.528\ \delta'^{18}O$, where $\delta'^{1x}O = \ln(^{x/16}R_{sample} / {}^{x/16}R_{standard})$, where x is 17 or 18. We report all δ and δ′ values in per mil (×10^3), and all $\Delta'^{17}O$ values in per meg (×10^6). This definition of $\Delta'^{17}O$ is equivalent to the '^{17}O-excess' parameter commonly used in the hydrological literature.

Recently, Guo and Zhou (2019a,b) have predicted from theory that kinetic fractionation may impart materials like speleothems and corals with distinct triple oxygen isotope compositions that testify to the extent of isotopic disequilibrium during mineralization.

1529-6466/21/0086-0013$05.00 (print)
1943-2666/21/0086-0013$05.00 (online)
http://dx.doi.org/10.2138/rmg.2021.86.13

As such, the continents are emerging as a particularly fruitful area of application for triple oxygen isotope studies, with $\Delta'^{17}O$ values strongly influenced by evaporation, possibly influenced by kinetic fractionation during mineralization, and, for organisms with waters of respiration comprising a large fraction of their overall water budget, by the unique $\Delta'^{17}O$ values of atmospheric O_2. Triple oxygen isotopes are potentially useful in systems ranging from lakes to soils to caves to plants to animals. At the time of this writing, very little information exists for soils and caves, so we focus our review on lakes, animal body waters, plant waters, and on the isotopic compositions of carbonates and bioapatites forming in natural waters and animals, respectively.

Precipitation (rain, snow) is the source of water on the continents, and thus is the triple oxygen isotope 'starting point' for all of these systems. The triple oxygen isotope compositions of continental carbonates and biological apatites are, to first-order, controlled by the isotopic compositions of their parent waters (e.g., lake water, animal body water). Therefore, much of this chapter focuses on the triple oxygen isotope compositions of natural waters and body water. The format for this discussion is to model the triple oxygen isotope evolution of water beginning with evaporation from the oceans, followed by Rayleigh distillation and production of continental precipitation, evaporative modification of this precipitation on the continents, and the triple oxygen isotope compositions of animals and plants that are sustained by this precipitation. All along this journey, we present the basic governing equations for modeling isotopic compositions, and we present observed triple oxygen isotope data in the context of these models. As much as possible, we present the model predictions and data in the form of $\Delta'^{17}O$ versus $\delta^{18}O$ bivariate plots, keeping the axis ranges uniform to give the reader a better context for the comparative absolute values and variability from one system to another.

Useful application of triple oxygen isotopes in paleoclimate depends on the ability to determine the triple oxygen isotope compositions of common minerals such as carbonates and apatites to high precision and accuracy. Following our discussion of natural and biological waters, we review the exciting developments of the past decade with respect to the analysis of carbonates and apatites and summarize the current state of inter-laboratory reproducibility. We examine the existing knowledge of key fractionation exponents for carbonate–water fractionation and fractionation during acid digestion.

We conclude the chapter by highlighting gaps in knowledge and opportunities for future research. Throughout this chapter, we use isotopic nomenclature as described in Miller and Pack (2021, this volume).

METEORIC WATERS

Evaporation from the oceans

The oceans are the dominant source of water vapor to the atmosphere. The triple oxygen isotope composition of the oceans is $\delta^{18}O \sim 0‰$, $\Delta'^{17}O = -5$ per meg (Luz and Barkan 2010), From this point of origin, there are four principle factors that determine the isotopic composition R_E of the evaporation flux reaching the free atmosphere: 1) the (temperature-dependent) equilibrium isotope fractionation between liquid and vapor, α_{eq}; 2) the relative humidity of air, normalized to the surface temperature of the water, h_n; 3) the relative contributions of molecular diffusion and turbulence in transporting water vapor to the free atmosphere (embodied in the α_{diff} parameter), and 4) the isotopic composition of ambient atmospheric water vapor, R_a. The isotopic composition of the evaporative flux is given by:

$$R_E = \frac{\frac{R_w}{\alpha_{eq}} - hR_a}{\alpha_{diff}\left(1-h_n\right)} \quad (1)$$

For adaptation to triple oxygen isotopes, equations such as Equation (1) are used twice: first in the $^{18}O/^{16}O$ space to determine $^{18}/^{16}R_E$, and then in the $^{17}O/^{16}O$ space to determine $^{17/16}R_E$. For the latter, $^{17/16}\alpha$ values are computed from $^{18/16}\alpha$ values using appropriate fractionation exponents θ and the relation $\theta = \ln(^{17/16}\alpha)/\ln(^{18/16}\alpha)$. Then, $\delta^{17}O$ and $\delta^{18}O$ values are calculated from the R values using the appropriate R values for VSMOW, and from these the $\Delta'^{17}O$ value is calculated after converting $\delta^{1x}O$ values to $\delta'^{1x}O$ values.

As pointed out by Luz and Barkan (2010), the basic form of Equation (1) has been obtained from the standpoints of diffusion theory (Ehhalt and Knott 1965), kinetic theory (Criss 1999), and from a steady-state evaporation model (Cappa et al. 2003). We note that Equation (1) is a key equation for describing the isotopic evolution of evaporating bodies of water on land, as discussed in the next section. Equation (1) also arises from the Craig–Gordon linear-resistance model (Craig and Gordon 1965; see also Gat 1996, and Horita et al. 2008), which envisions an equilibrium vapor layer immediately overlying the liquid water surface, with further fractionation resulting from transport of this equilibrium vapor to the free atmosphere via a combination of molecular diffusion and turbulence. Pure molecular diffusion carries fractionations of $^{18/16}\alpha = 1.028$ and $\theta = 0.5185$ (as determined experimentally by Merlivat 1978 and Barkan and Luz 2007, respectively; see discussion in the latter and also Horita et al. (2008) and Cappa et al. (2003) regarding discrepancies between experimentally-derived $^{18/16}\alpha$ values and the theoretical value, 1.032, and possible explanations for these discrepancies). Thus, in the $\lambda = 0.528$ reference frame, diffusion-dominated evaporation involves a substantially higher $\Delta'^{17}O$ value for the vapor, and, by mass balance, a corresponding lowering of $\Delta'^{17}O$ of the residual liquid (Fig. 1), while turbulence-dominated evaporation will result in less elevated $\Delta'^{17}O$ of vapors and more modest lowering of $\Delta'^{17}O$ in the residual liquid. To first-order, turbulence scales with windiness: in stagnant air, which occurs inside of leaves and soils, and can be achieved in laboratory experiments, $^{18/16}\alpha_{diff}$ approaches the 1.028 limit for

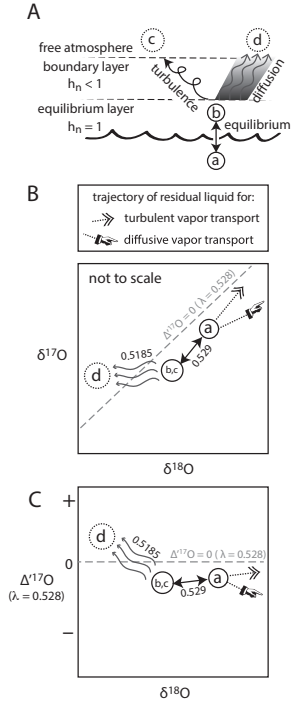

Figure 1. Schematic depiction of triple oxygen isotope fractionation during evaporation. A. In the Craig–Gordon model, an equilibrium layer of water vapor **(b)** with $h_n = 1$ lies in contact with the water surface **(a)**. From here, vapor is transported to the atmosphere via a combination of turbulent transport, which is non-fractionating, and molecular diffusion, which is fractionating. The vapor produced by each process are noted by **(c)** and **(d)** in the figure. Note that the Craig–Gordon model, these two processes are linked in series and not in parallel as this simplified endmember schematic might imply. The schematic also does not depict isotopic exchange with ambient water vapor. **B, C**. Evaporation in triple oxygen isotope space, showing the relative trajectories for vapor and residual liquid in the turbulent transport endmember (**c** and **double arrow**, respectively), and for vapor and residual liquid in the diffusion endmember (**d**, **hand pointer**, respectively). Liquid **a** and vapor **b** are linked by the equilibrium fractionation exponent $\theta_{eq} = 0.529$ (Barkan and Luz 2005), and molecular diffusion (**b** to **d**) has a θ value of 0.5185 (Barkan and Luz 2007).

molecular diffusion. Combined with the θ_{diff} value of 0.5185, this leads to highly-modified $\Delta'^{17}O$ values of vapor and residual liquid. In windy conditions, turbulence develops, $^{18/16}\alpha_{diff}$ values become substantially smaller, and $\Delta'^{17}O$ values are less extreme even though the θ_{diff} value is unchanged. This is because deviations in $\Delta'^{17}O$ are dependent both on the magnitude of isotopic fraction ($^{18/16}\alpha$) and the numerical difference between the θ value of the fractionation and the reference frame slope (here 0.528) (Guo and Zhou 2019a):

$$\Delta\Delta'^{17}O_{A-B} = \left(\theta_{A-B} - 0.528\right) \times \ln\left(^{18/16}\alpha_{A-B}\right) \quad (2)$$

where $\Delta\Delta'^{17}O_{A-B}$ is the difference in $\Delta'^{17}O$ between two phases that exchange isotopes, θ_{A-B} is the fractionation exponent between these two phases, and $^{18/16}\alpha_{A-B}$ is the fractionation factor between these phases.

A simplifying assumption when treating evaporation of seawater is the 'closure assumption' (Merlivat and Jouzel 1979), which assumes that the only source of water vapor in the atmosphere is evaporation from the oceans, so that $R_E = R_a$. Inserting this equivalency into Equation (1) gives:

$$R_E = R_w \Big/ \alpha_{eq}\left(\alpha_{diff}\left(1 - h_n\right) + h_n\right) \quad (3)$$

Uemura et al. (2010) determined a value of $^{18/16}\alpha_{diff} = 1.008$ for evaporation from the South Indian and Southern Oceans, meaning that the fractionation during vapor transport is closer to the turbulence endmember ($^{18/16}\alpha_{diff} = 1$) than it is to the molecular diffusion endmember ($^{18/16}\alpha_{diff} = 1.028$). Using $^{18/16}\alpha_{diff} = 1.008$, we use Equation (3) to model the isotopic compositions of marine vapors and the theoretical initial condensates of those vapors for h_n of 0.5, 0.7 and 0.9 (Fig. 2). As can be seen, lower relative humidity results in higher $\Delta'^{17}O$ values of the water vapor flux, which ultimately will lead to higher $\Delta'^{17}O$ values of condensates, including precipitation on the continents. This arises from a combination of enhanced diffusion due to the greater water vapor concentration gradient between the boundary layer and free atmosphere, as well as the decreased influence of ambient atmospheric water vapor at lower relative humidity, in terms of isotopic exchange. In general, the positive $\Delta'^{17}O$ values of global precipitation can be attributed to (1) the influence of molecular diffusion during evaporation from the oceans, and (2) the fact that condensation has a θ value of 0.529, slightly steeper than the 0.528 reference slope, which imparts condensates with a slightly higher $\Delta'^{17}O$ value than the parent vapors (Fig. 2B).

Rayleigh distillation and the triple oxygen isotope meteoric water line

Rayleigh distillation theory has stood the test of time as the explanation for the first-order features of the $\delta D - \delta^{18}O$ global meteoric water line (GMWL) (Craig 1961; Dansgaard 1964), and Rayleigh theory also accurately predicts the general features of the triple oxygen isotope GMWL (Luz and Barkan 2010). The Rayleigh equation for water vapor in a condensing parcel of air can be given as:

$$R_f = R_0 f^{(\alpha_{eq} - 1)} \quad (4)$$

where f is fraction of water vapor that remains in a parcel of air relative to the initial amount of water vapor, R_0 is the initial isotopic composition of water vapor in the parcel, R_f is the instantaneous isotopic composition of vapor when fraction f remains, and α_{eq} is the equilibrium fractionation between liquid water and water vapor. The α_{diff} parameter does not appear in Equation (4) because the condensation of liquid requires that relative humidity is 100%; hence there is no concentration gradient in water vapor, and therefore no net transport by molecular diffusion. The only isotopic fractionation at play is equilibrium between liquid water and water vapor, which carries a fractionation exponent of 0.529 (Barkan and Luz 2005).

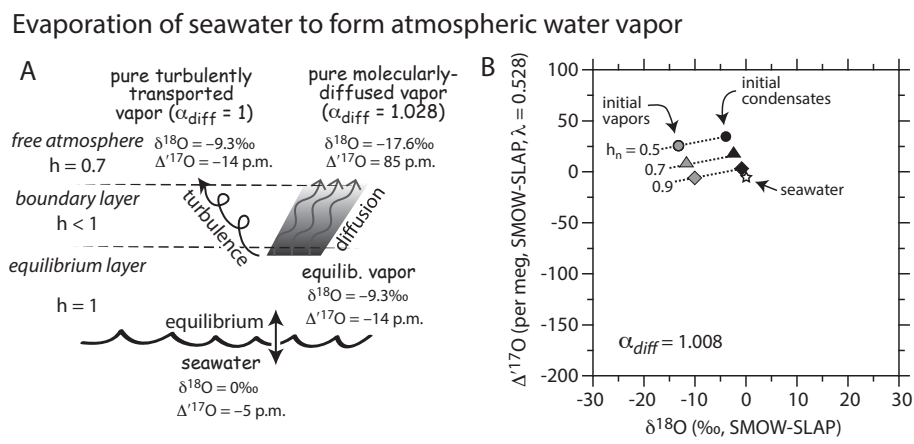

Figure 2. Evaporation of seawater to form atmospheric water vapor. **A.** As in Figure 1A, but showing triple oxygen isotopic compositions for equilibrium vapors, the pure turbulently-transported vapor endmember, and the pure molecularly-diffused vapor endmember. These values were calculated for 25 °C using $^{18/16}\alpha_{eq}$ = 1.0093 (Majoube 1971), θ_{eq} = 0.529 (Barkan and Luz 2005), $^{18/16}\alpha_{diff}$ = 1.028 (Merlivat and Jouzel 1978) and θ_{diff} = 0.5185 (Barkan and Luz 2007). **B.** Triple oxygen isotope compositions of initial vapors calculated using Equation (3), and initial condensates from those vapors for different humidities. Here we use $^{18/16}\alpha_{diff}$ = 1.008, the best-fit value for marine vapors in the South Indian and Southern Oceans observed by Uemura et al. 2010. Abbreviation: p. m. : per meg.

This commonly leads to the mistaken assumption that the 'theoretical' slope of the triple oxygen isotope GMWL is also 0.529. However, evaluation of Equation (4) (see Fig. 3) shows that this is not the case: for constant values of $^{18/16}\alpha_{eq}$ = 1.0093 (Majoube 1971; 25 °C) and θ_{eq} = 0.529, the GMWL slope is 0.5278. If $^{18/16}\alpha_{eq}$ is allowed to increase in a systematic manner as *f* decreases (as must be the case, because decreasing *f* can only be driven by decreasing temperatures, which drives saturation and hence condensation), then slightly lower slopes are observed. Note that θ_{eq} is not observed to vary significantly over Earth surface temperatures (Barkan and Luz 2005). Luz and Barkan (2010) showed that the slope γ of the GMWL in a pure Rayleigh distillation model can be given by:

$$\gamma = \frac{^{17}\alpha_{eq} - 1}{^{18}\alpha_{eq} - 1} \tag{5}$$

with the slope ranging from 0.5275 to 0.5279 over the temperature range 0–30 °C.

The canonical slope of 0.528 for the GMWL historically arises from Equation (5) and from the initial observations of global meteoric water triple oxygen isotope compositions (Landais et al. 2008; Luz and Barkan 2010). However, considerable additional data have been published since 2010, and it is now clear (e.g., Sharp et al. 2018) that the slope is lower in tropical + temperate climates. Figure 4 presents an up-to-date compilation from the literature, excluding polar regions where $\delta^{18}O < -30‰$, and screened for waters subject to evaporation (lakes and ponds) (i.e., it is a precipitation dataset, not a meteoric water data set). Additionally, the data are weighted where possible for amount of precipitation, which includes the use of weekly- or monthly-averages over individual precipitation event values. Such weighting is important for understanding the water inputs for lakes, soil waters, and animal body waters, because we are interested in the amount-weighted isotopic composition of waters available to these systems. For this dataset, the slope is 0.5272, with a clear tendency to 'curve' towards lower $\Delta'^{17}O$ values when $\delta^{18}O$ is ~ –10‰ and higher. The mechanism(s) for lower $\Delta'^{17}O$ values at higher $\delta^{18}O$ are as yet resolved, but following theoretical considerations presented above,

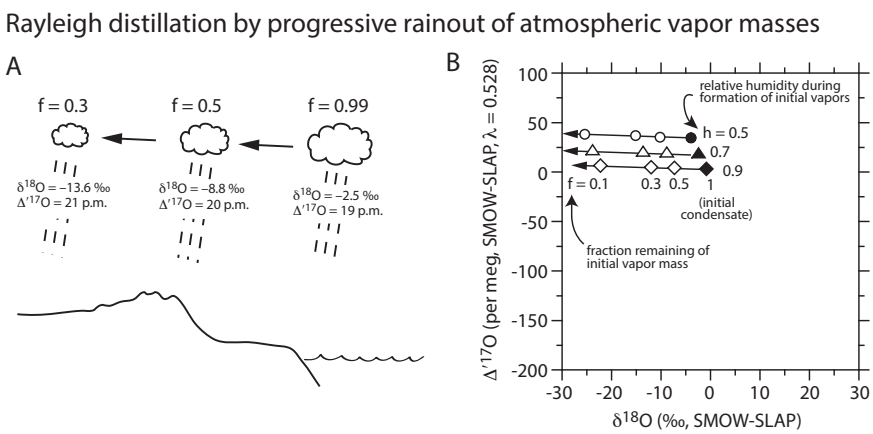

Figure 3. Rayleigh distillation in triple oxygen isotope space. **A.** Schematic view of the process, with isotopic compositions given for fractions remaining of initial vapor mass $f = 0.99$, 0.5, and 0.3. **B.** The process in triple oxygen isotope space, modeled using Equation (4) for each of the three initial vapors shown in Figure 2B. Note that this figure (3B) portrays the compositions of the condensates (i.e., precipitation). Calculated using $^{18/16}\alpha_{eq} = 1.0093$ and $\theta_{eq} = 0.529$.

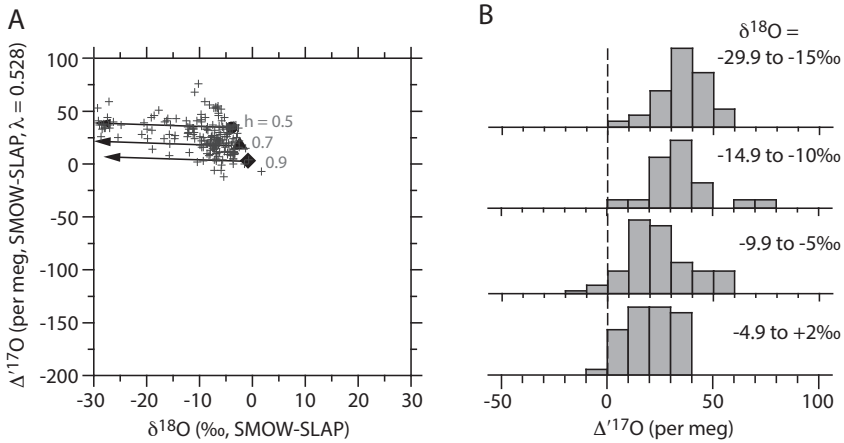

Figure 4. Observed triple oxygen isotope compositions of global precipitation. **A.** Precipitation values (**+ signs**) plotted in the context of the Rayleigh distillation models presented in Figure 3. **B.** Relative frequency of $\Delta'^{17}O$ values in 10 per meg bins, grouped according to $\delta^{18}O$ range. This illustrates the clear shift towards lower $\Delta'^{17}O$ values with higher $\delta^{18}O$. $\Delta'^{17}O$ values of precipitation lower than 0 per meg and higher than 50 per meg are uncommon. Data are from Landais et al. (2008, 2010, 2012), Luz and Barkan (2010), Li et al. (2015), Surma et al. (2015), Tian et al. (2018), Passey and Ji (2019), and Uechi and Uemura (2019).

viable mechanisms include higher relative humidity or a greater degree of turbulent transport of water vapor during evaporation from the oceans, or increased re-evaporation of rainfall and surface waters in settings where $\delta^{18}O$ is high.

Evaporation from isolated bodies of water

Precipitation is subject to re-evaporation following condensation, which takes place during the journey of water back to the oceans. For isolated bodies of water evaporating into a humid atmosphere (e.g., pan evaporation, raindrop re-evaporation), the isotopic ratio of the residual water can be modeled as Stewart (1975), Criss (1999), Surma et al. (2015):

$$R_w = f^u \left(R_{w,initial} - R_{w,ss} \right) + R_{w,ss} \tag{6}$$

where R_w is the isotope ratio of the water body, f is the fraction of water remaining, $R_{w,initial}$ is the initial isotope ratio of the water, and where the exponent u is given by:

$$u = \frac{1 - \alpha_{eq}\alpha_{diff}\left(1-h\right)}{\alpha_{eq}\alpha_{diff}\left(1-h\right)} \tag{7}$$

and with $R_{w,ss}$, the steady-state isotopic composition that the water body may reach at low f, given by:

$$R_{w,ss} = \frac{\alpha_{eq} h_n R_a}{1 - \alpha_{eq}\alpha_{diff}\left(1-h_n\right)} \tag{8}$$

where atmospheric vapor is commonly assumed to be in equilibrium with the initial, unevaporated water ($R_a = R_I/\alpha_{eq}$). These equations predict that $\Delta'^{17}O$ of the water body decreases as evaporation proceeds (Fig. 5B). At higher h_n, the evaporation trajectory is 'steeper' in a $\delta^{18}O$ vs $\Delta'^{17}O$ plot (lower effective λ value), but the steady-state $\Delta'^{17}O$ and $\delta^{18}O$ values are higher and lower, respectively, than for low h_n. In other words, the lowest $\Delta'^{17}O$ values are obtained when f is low, h_n is low, and (not illustrated in Fig. 5B), when $^{18/16}\alpha_{diff}$ values are high (i.e., towards the 1.028 endmember). The predictions of Equations (6–8) are supported by a number of laboratory evaporation experiments (e.g., Luz and Barkan 2010; Surma et al. 2015; Li et al. 2017), and by data from natural evaporating ponds (Surma et al. 2015, 2018). Equations (6–8) are also used as a basis for modeling the evolution of evaporating raindrops, which is a more complicated scenario because R_a is itself influenced by evaporation from the raindrop, because α_{diff} may vary according to the size and velocity of the raindrop, and because temperature may change as the raindrop falls. For detailed treatments of evaporating rainfall, the reader is referred to Landais et al. (2010), Bony et al. (2008), and references therein.

Closed-basin and throughflow lakes

Lakes are generally not isolated bodies of water, but rather have inflows of water (rivers, groundwater, direct precipitation), outflows (rivers, groundwater), and evaporation. Following Criss (1999), the isotopic mass balance of a lake can be described by:

$$\frac{\partial(VR_{lw})}{\partial t} = IR_I - OR_O - ER_E \tag{9}$$

where V is lake volume, R_{lw} is the isotope ratio of lake water, I is the inflow flux (which combines influx from rivers, groundwater, and precipitation), R_I is the inflow isotope ratio, O is the outflow flux, R_O is the outflow isotope ratio, E is the evaporation flux, and R_E is the isotope ratio of water lost by evaporation. For a well-mixed lake with a constant volume and in isotopic steady state, Equation (9) becomes:

$$I_I R_I = OR_O + ER_E \tag{10}$$

In a closed basin lake at isotopic steady state, the isotope ratio of water leaving the lake by evaporation must be equivalent to the isotope ratio of the water flux into the lake ($R_E = R_I$). Inserting thie equivalency into Equation (1) and solving for R_w (which we rename R_{lw}) gives:

$$R_{lw} = \alpha_{eq}\alpha_{diff} R_I \left(1 - h_n\right) + \alpha_{eq} h R_a \tag{11}$$

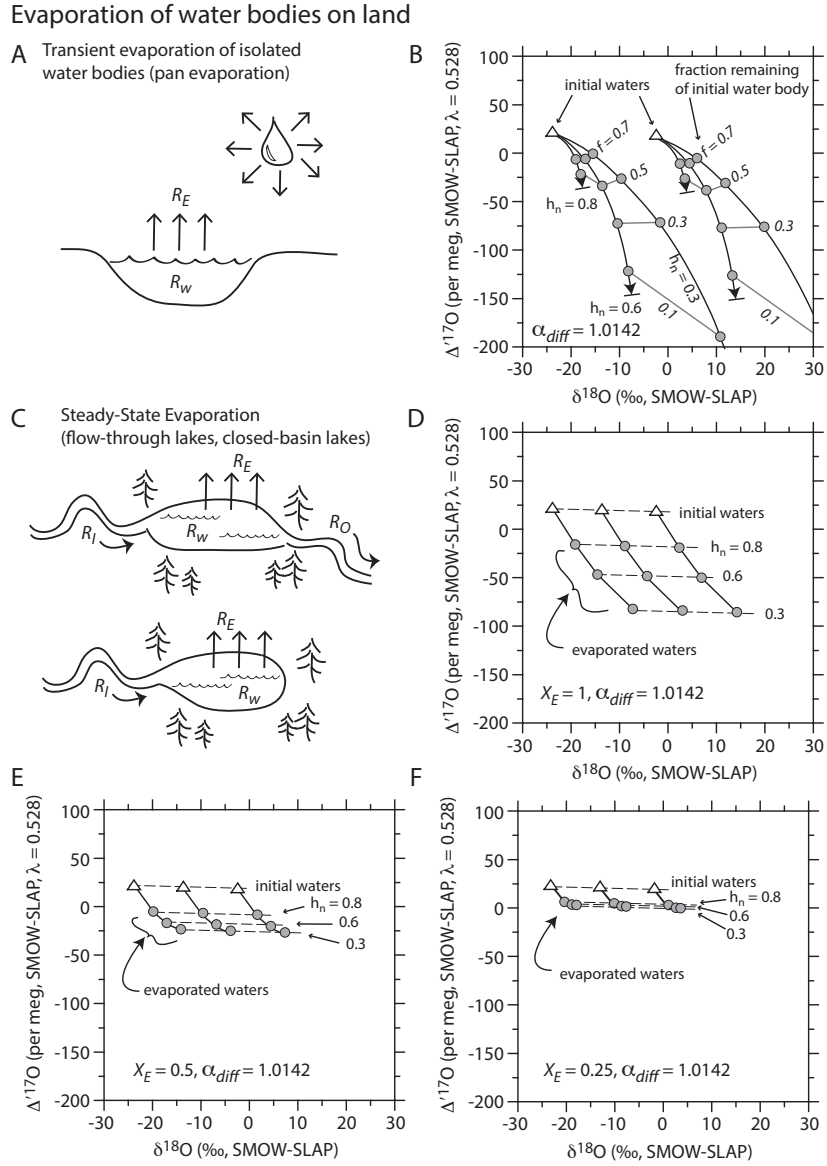

Figure 5. Models of open pan and steady-state evaporation, starting with initial waters modeled in Figure 3 for $h_n = 0.7$. **A, B**. Transient (**open pan**) evaporation, modeled using Equations (6–8) for a range of h_n, and constant $^{18/16}\alpha_{diff} = 1.0142$. Initial waters are shown by triangles, and isotopic compositions at different stages in the progress of evaporation are shown by circles. Fractional extents of evaporation (*f*) are noted in italicized text. The **curved solid arrows** show the evaporation trajectories for different values of h_n, and the endpoints of the arrows for $h_n = 0.8$ and $h_n = 0.6$ are the final, steady state compositions of the water (the steady-state compositions for $h_n = 0.3$ fall off the plot). **Sub-horizontal gray lines** connect the common fractional extents of evaporation at different h_n. **C–F.** Steady-state isotopic compositions calculated using Equation (16) for closed basin lakes ($X_E = 1$; **D, E**) and a flow through lakes ($X_E = 0.5, 0.25$). Note that in contrast to Figure 5B, the **solid angled lines** are not evaporation trajectories, but rather connect the steady-state isotopic compositions for evaporation of the same initial water compositions at different relative humidity. The models in **D, E,** and **F** differ only in X_E, illustrating the sensitivity to this parameter. For all models, $^{18/16}\alpha_{eq} = 1.0093$, $\theta_{eq} = 0.529$, $\theta_{diff} = 0.5185$, and R_a is assumed to be in isotopic equilibrium with the initial (inflow) waters.

For a throughflow lake at steady-state, we can denote the fraction of water leaving the lake by evaporation as:

$$X_E = \frac{E}{I} \tag{12}$$

Combining Equation (12) with Equation (10) gives:

$$X_E R_E + \left(1 - X_E\right) R_o = R_I \tag{13}$$

For a well-mixed lake, $R_O = R_{lw}$ (i.e., the outflow composition is the same as the lake composition). Inserting this equivalency into Equation (13) and solving for R_E gives:

$$R_E = \frac{R_I - \left(1 - X_E\right) R_{lw}}{X_E} \tag{14}$$

Combining this equation with Equation (1) gives:

$$\frac{R_I - \left(1 - X_E\right) R_{lw}}{X_E} = \frac{R_w - \alpha_{eq} h_n R_a}{\alpha_{eq} \alpha_{diff} \left(1 - h_n\right)} \tag{15}$$

Finally, multiplying both sides by the denominator on the right hand side and solving for R_{lw} gives a general solution for both closed basin lakes ($X_E = 1$) and flowthrough lakes ($X_E < 1$) (cf., Criss 1999, Eqn. 4.46c, where Criss' $\alpha^0_{evap} = \alpha_{eq}\alpha_{diff}$):

$$R_{lw} = \frac{\alpha_{eq} \alpha_{diff} \left(1 - h_n\right) R_I + X_E h_n \alpha_{eq} R_a}{\alpha_{eq} \alpha_{diff} \left(1 - h_n\right)\left(1 - X_E\right) + X_E} \tag{16}$$

Figures 5D–F show the predictions of this equation, evaluated for a range of initial water oxygen isotopic compositions, relative humidities, and X_E values, and assuming that atmospheric vapor is in equilibrium with inflow waters ($R_a = R_I/\alpha_{eq}$). Note that these are steady-state isotopic compositions, and not transient evaporation trajectories as shown for pan evaporation in Figure 5B. Figures 5D–F show that $\Delta'^{17}O$ is most changed when h_n is low, and fraction of evaporation from the lake (X_E) is high.

The models shown in Figure 5 all hold R_a and α_{diff} constant, whereas lake water $\Delta'^{17}O$ and $\delta^{18}O$ values are highly sensitive to these parameters (Fig. 6). The sensitivity to R_a is greatest at high relative humidity (Fig. 6A), in part because humid air holds more water vapor that can exchange with surface waters. The sensitivity to α_{diff} is greatest at low relative humidity (Fig. 6B) due to the steeper water vapor concentration gradient between the boundary layer and the free atmosphere at low humidity.

A final factor is the influence of atmospheric water vapor derived from evaporation of the the water body itself (e.g., Benson and White 1994; Gat et al. 1994; Gat 1996; Gibson et al. 2016). Here, Equation (16) can be modified to (Passey and Ji 2019):

$$R_{lw} = \frac{\alpha_{eq} R_I \left[\alpha_{diff}\left(1 - h_n\right) + h_n\left(1 - F\right)\right] + \alpha_{eq} h_n X_E R_a F}{X_E + \alpha_{eq}\left[1 - X_E\right]\left[\alpha_{diff}\left(1 - h_n\right) + h_n\left(1 - F\right)\right]} \tag{17}$$

where F is the fraction of water derived from regional sources upwind of the lake, and $(1 - F)$ is the fraction of moisture derived from the lake (note that this equation does not explicitly

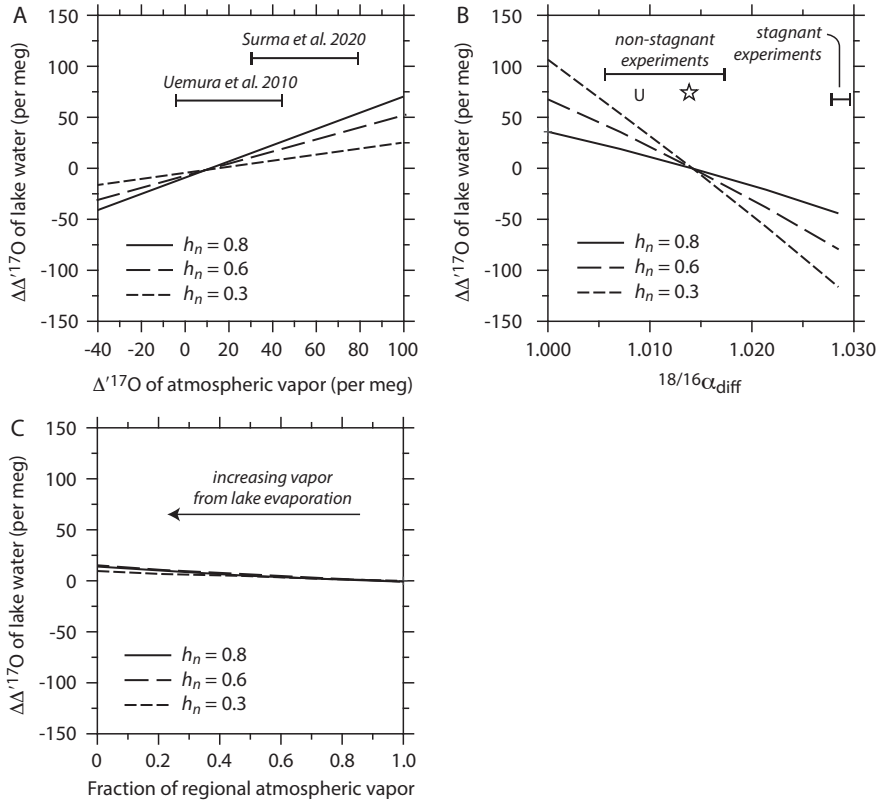

Figure 6. Sensitivity of closed-basin lake water $\Delta'^{17}O$ values to changes in $\Delta'^{17}O$ of atmospheric vapor (**A**), $^{18/16}\alpha_{diff}$ (**B**), and fraction of atmospheric vapor derived from regional sources in equilibrium with precipitation (**C**). In all figures, the vertical axis reflects the difference in $\Delta'^{17}O$ compared to the base model in Figure 5D. The **horizontal brackets in (A)** represent the range of atmospheric water vapor values observed in the marine environment by Uemura et al. (2010), and in the European Alps by Surma et al. (2021, this volume). The **horizontal brackets in (B)** represent the range of values for laboratory experiments where air above the evaporating water was stagnant and non-stagnant, as compiled by Horita et al. (2008; Table 2). The 'U' shows the best-fit $^{18/16}\alpha_{diff}$ value for marine evaporation determined by Uemura et al. (2010), and the star show the 'canonical' 1.014 value commonly assumed for continental evaporation. In (**C**), a fractional value of 0 means that all atmospheric vapor over a lake is derived from evaporation from the lake itself, while a value of 1 means that all atmospheric vapor is derived from regional sources in equilibrium with precipitation.

account for the influence of lake evaporation on h_n). F can approach 0 for lakes in arid climates (e.g., Pyramid Lake, Nevada; Benson and White 1994), while Gat et al. (1994) estimate that F ranges between 0.84 and 0.95 for the more humid Great Lakes of North America. In general, changes in F have a smaller influence on the isotopic composition of lake water than do changes in R_a and α_{diff} (Fig. 6C).

Special considerations and case studies

The collective results from modeling and field studies of modern lakes and ponds (Luz and Barkan 2010; Surma et al. 2015, 2018; Gázquez et al. 2018; Passey and Ji 2019) suggest a number of approaches and challenges for using triple oxygen isotopes in modern and past lakes. The essential challenge to quantitative paleoclimate reconstruction in lacustrine environments is that there are six variables in Equation (17) (R_I, R_a, h_n, X_E, α_{diff}, F), whereas only two isotope ratios ($^{17}O/^{16}O$, $^{18}O/^{16}O$) are measured. How then can we reliably reconstruct any of

the remaining variables of this underconstrained system? Fortunately, there is a hierarchy in sensitivity to these variables (approximately $X_E > h_n > \alpha_{diff} > R_a > R_I > F$)), so a lack of direct constraints on e.g., R_I and F may not greatly hinder interpretations in certain cases. Here we discuss some additional considerations, not mutually exclusive, for sound interpretation of triple oxygen isotope data, and do so in the context of published results where appropriate.

Qualitative indicator of evaporation. Authigenic minerals are commonly used to reconstruct past climates or past surface elevation in tectonic settings (e.g. Rowley and Garzione 2007), and both approaches generally assume that the reconstructed $\delta^{18}O$ values are reflective of primary precipitation, with recognition that evaporation can throw interpretations into serious error. Despite the large number of variables in Equation (17), all scenarios of evaporation lead to lowering of $\Delta'^{17}O$ of surface waters, save perhaps for cases where $\Delta'^{17}O$ of atmospheric vapor is unusually high. $\Delta'^{17}O$ values lower than 0 per meg are uncommon for unevaporated precipitation (Fig. 4), whereas values lower than 0 per meg are common for evaporated waters (Surma et al. 2015, 2018; Gázquez et al. 2018; Passey and Ji 2019). Therefore, at the most basic level, triple oxygen isotope analysis will reveal whether the mineral parent waters are likely to have been modified by evaporation ($\Delta'^{17}O < \sim 0$ per meg), and thus are unsuitable for interpretation in terms of $\delta^{18}O$ of pristine precipitation. Low $\Delta'^{17}O$ values will also qualitatively indicate hydrological and climatic conditions conducive for appreciable evaporation (high X_E, low h_n).

Directional constraints. As $\Delta'^{17}O$ values of lake water becomes lower, the parameter space that can account for the values diminishes. For example, $\Delta'^{17}O$ values of ~ 0 per meg are consistent with very low relative humidity but little net evaporation (Figs. 5B, F), as well as high relative humidity and appreciable evaporation (Figs. 5D, E). On the other hand, $\Delta'^{17}O$ values of lower than ~ –50 per meg only occur when net evaporation is > 50 %, and relative humidity is ~0.6 or lower (Figs. 5B, D, E). Therefore, although $\Delta'^{17}O$ data may not permit precise reconstruction of parameters such as h_n or X_E, they can be used to rule out portions of the parameter space.

Independently-constrained variables. Gázquez et al. (2018) presented the first application of lacustrine triple oxygen isotope systematics to the paleoclimate record. Following methods described by Gázquez et al. (2017), they analyzed triple oxygen isotopes and hydrogen isotopes in waters of hydration of lacustrine gypsum extending back ~15 kyr at Lake Estanya in Spain. Given that gypsum formation requires closed-basin or nearly closed basin settings, gypsum-based studies are able isolate X_E to values near 1. Gázquez et al. (2018) then used a Monte-Carlo approach to randomly vary the other parameters in an equation similar to Equation (17), and then selected only the parameter sets that correctly predicted the measured triple oxygen and deuterium isotopic compositions of the gypsum hydration waters. This approach allowed them to constrain changes in normalized atmospheric relative humidity over this time interval, and to robustly conclude that h_n during the Younger Dryas was substantially lower than during the late Holocene (by ~20% or more on the 0–100% h_n scale; see their Fig. 5). Their inferred absolute values of h_n for the Younger Dryas and late Holocene are more dependent on assumptions made about the $^{18/16}\alpha_{diff}$ parameter (see their Fig. 5c).

Passey and Ji (2019) sought to examine the predictions of Equation (17) by studying modern lakes where many of the free parameters in Equation (17) could be constrained. They examined three closed-basin lakes ($X_E = 1$) (Great Salt Lake, Mono Lake, Pyramid Lake), each having three or fewer major inflowing rivers that account for the vast majority of water input into the lake, hence allowing R_I to be constrained. Additionally, detailed climatologies exist for this region, including monthly relative humidity and potential evapotranspiration, which together allow for estimates of the effective relative humidity weighted to the months with highest evaporation (here, the summer months). For Great Salt Lake, Pyramid Lake, and Mono Lake, the evaporation-weighted relative humidities are 43%, 42%, and 44%, respectively, based on data from New et al. (2002). A compilation of monthly lake water and air temperature data from 88 lakes globally in Hren and Sheldon (2012) shows that summer water temperatures are generally

similar or slightly warmer (by a few degrees) than summer air temperature; thus the water surface temperature normalized relative humidities (h_n) are likely similar to, or lower than, the free air relative humidities reported above. Consequently, the major unconstrained parameters for the closed-basin lakes was $^{18/16}\alpha_{diff}$ and R_a. $^{18/16}\alpha_{diff}$ is commonly assumed to be ~ 1.014 for continental lakes (e.g., Gat 1996; Horita et al. 2008; Jasechko et al. 2013; Gibson et al. 2016). Figure 7 shows the results for these lakes in the context of models where $^{18/16}\alpha_{diff}$ = 1.0142 and 1.0086. For the $^{18/16}\alpha_{diff}$ = 1.0142 models, the relative humidities required to explain the observed lake water compositions are unrealistically high, whereas the $^{18/16}\alpha_{diff}$ = 1.0086 models achieve a much better fit to the known relative humidities and isotopic compositions. Alternatively, models where $^{18/16}\alpha_{diff}$ = 1.0142, but R_a is higher (60 per meg instead of 12 per meg) also better predict the observed data within the constraints of known h_n and X_E.

There is good evidence that both R_a and $^{18/16}\alpha_{diff}$ may depart from commonly assumed values. For example, Surma et al. (2021, this volume) show that continental vapors in the European Alps have substantially higher $\Delta'^{17}O$ than water vapors in equilibrium with local surface waters. The parameter $^{18/16}\alpha_{diff}$ can theoretically range by 28‰ (!) (1 to 1.028), and

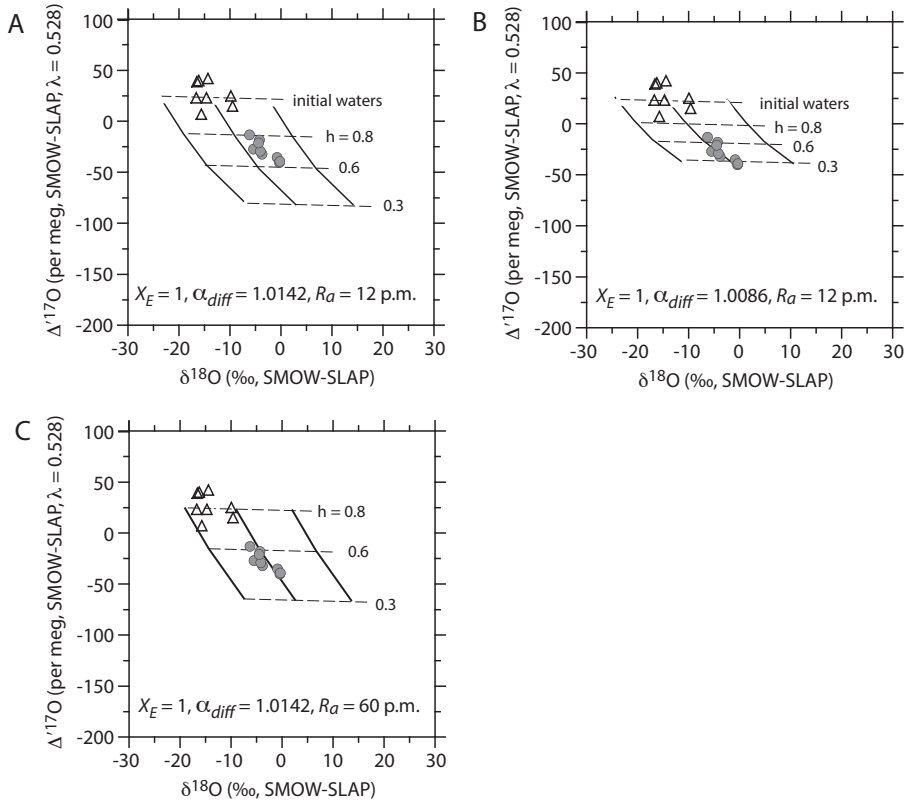

Figure 7. Western United States closed-basin lakes and inflow rivers (Mono Lake, Pyramid Lake, and Great Salt Lake). **A**. Inflow rivers (**triangles**) and lake waters (**gray circles**), plotted in the context of the model (Eqn. 16) from Figure 5D, where $^{18/16}\alpha_{diff}$ = 1.0142. **Solid lines** connect waters with initial (unevaporated) isotopic compositions shown in Figure 3b for h_n = 0.7. **B.** As (A), but plotted in the context of models for $^{18/16}\alpha_{diff}$ = 1.0086. The latter models are more realistic, given that potential evapotranspiration-weighted relative humidity for these lakes is ~40 – 45%. C. As (A), but with R_a = 60 per meg instead of 12 per meg. The significance of the value of 60 per meg is that it is in the upper ~1/3 of the range of values reported for the European Alps by Surma et al. (2021, this volume). Data are from Passey and Ji (2019).

the wide range of values observed in experimental studies (see Fig. 6), and the closed-basin results from Passey and Ji (2019) suggest that variation for natural lakes may be greater than commonly assumed. Moving forward, there is a need better characterization of R_a and $^{18/16}\alpha_{diff}$ parameter across the range of continental evaporation scenarios.

Exploiting parameter-insensitive trajectories. Surma et al. (2018) explored evaporation trajectories in triple oxygen isotope space using a combination of modeling and observational results from the Atacama Desert, Chile. They suggest that in many cases, the shape of the evaporation trajectory for flow-through lakes in $\Delta'^{17}O$ versus $\delta^{18}O$ is insensitive to parameters such as h_n, α_{diff}, and temperature (their Figs. 4a–e), whereas the *extent* to which samples evolve along the trajectory is highly sensitive to X_E and h_n. However, variation in R_a can cause these trajectories to differ significantly (their Figs. 4f–h), and in cases of transient evaporation, the shape of the trajectory is strongly dependent on h_n (Fig. 5B of this chapter).

Alternatively, Passey and Ji (2019) used a Monte-Carlo approach to show that the evaporation slope λ_{lake} between unevaporated inflow waters and evaporated lake waters is relatively conservative despite the large number of variables in Equation (17). Thus, this slope is predictable and can be used to 'back-project' the composition of the evaporated lake water to the intersection with an assumed unevaporated triple oxygen isotope MWL. In other words, while the reconstructed triple oxygen isotope composition cannot be used to uniquely reconstruct individual parameters such as X_E and h_n, the data can be used to estimate the $\delta^{18}O$ value of unevaporated precipitation, which is an important goal in the isotopic reconstruction of past climates. The uncertainty is not insubstantial (generally a few per mil), but given that closed basin lakes can be elevated in $\delta^{18}O$ by 10–15‰ relative to unevaporated catchment precipitation, this level of error may be acceptable in many applications.

ANIMAL AND PLANT WATERS

Carbon and oxygen isotope analysis of vertebrate bioapatites is a cornerstone of reconstructing continental climate and paleoecology (Koch 1998; Kohn and Cerling 2002), but the unequivocal interpretation of oxygen isotope data has been hampered by the numerous competing factors that influence animal body water $\delta^{18}O$, and hence animal bioapatite $\delta^{18}O$ (e.g., Luz and Kolodny 1985; Ayliffe and Chivas 1990; Bryant and Froelich 1995; Kohn 1996; Levin et al. 2006; Blumenthal 2017). Evaporation is a key part of the water balance of many animals, in terms of the intake of evaporated waters (e.g., leaf waters, evaporated surface waters), and in terms of evaporation of water from the animal. Furthermore, in many animals, a substantial fraction of the O in body water comes from atmospheric O_2 via basic metabolic respiration (i.e., $CH_2O + O_2 \rightarrow CO_2 + H_2O$). Atmospheric O_2 has a highly distinctive $\Delta'^{17}O$ value of –434 ± 22 per meg (this is the average and standard deviation from studies analyzing tropospheric O_2 directly against the VSMOW2-SLAP scale: Barkan and Luz 2005, Pack et al. 2017; Wostbrock et al. 2020; cf., Pack 2021, this volume). Therefore, triple oxygen isotopes are uniquely suited for application to terrestrial vertebrates.

Andreas Pack's group at Georg August University of Göttingen have pioneered this emerging field (Gehler et al. 2011), focusing in particular on the prospect of reconstructing past carbon dioxide levels (Pack et al. 2013; Gehler et al. 2016), following on the sensitivity of the $\Delta'^{17}O$ of atmospheric O_2 to pCO_2 (Luz et al. 1999; Bao et al. 2008; Cao and Bao 2013; Young et al. 2014; Brinjikji and Lyons 2021, this volume; Pack 2021, this volume). O_2-derived oxygen in body water is diluted by other sources of oxygen to animals, and the isotopic composition of body water is further modified by isotopic fractionations associated with both inputs and outputs of oxygen-bearing species. Therefore, accurate isotope mass balance body water models are necessary for meaningful interpretation of triple oxygen isotope data in terms of reconstructing the $\Delta'^{17}O$ of atmospheric O_2, and also of reconstructing

the paleoclimatic and paleoecological significance of data. Pack et al. (2013) developed a triple oxygen isotope model based on the $\delta^{18}O$ model of Bryant and Froelich (1995), where the input and output fluxes are scaled to body mass. In the model, the relative proportion of O_2-derived oxygen decreases as body mass increases, which follows the observation that smaller animals are often more independent of water (i.e., require less drinking water) than larger animals. Whiteman et al. (2019) developed a model that similarly ties the relative proportion of O_2-derived oxygen to metabolic rate and hence body mass.

Figure 8 shows the currently available triple oxygen isotope data for modern vertebrates, plotted as a function of body mass (Pack et al. 2013; Passey et al. 2014; Whiteman et al. 2019). The data support a general trend with body mass, with smaller animals having lower $\Delta'^{17}O$ values, which is consistent with a higher fraction of O_2-derived oxygen, given that the $\Delta'^{17}O$ of O_2 is ~ –0.43‰. However, Figure 8 also shows that there is a large degree of variation in $\Delta'^{17}O$ that is independent of body mass, and that the degree of variation at a fixed body mass can rival or exceed the difference in $\Delta'^{17}O$ between the low and high ends of the regression lines. This is not surprising, given that previous studies have shown that $\delta^{18}O$ may vary greatly according to factors unrelated to body mass, such as relative humidity (Ayliffe and Chivas 1990; Luz et al. 1990) and leaf-water intake (Levin et al. 2006; Blumenthal et al. 2017).

Here we explore such "mass independent" influences on the triple oxygen isotope compositions of animals. We make use of a triple oxygen isotope version (Hu 2016) of the $\delta^{18}O$ model developed by Kohn (1996), which allows for detailed adjustments in fluxes such as plant leaf water (fractionated by evaporation), stem/root water (unfractionated relative to soil water), the carbohydrate / protein / fat composition of diet (as each has a different stoichiometric demand for O_2 during respiration), and the relative effluxes of urinary, fecal, and sweat water (unfractionated relative to body water) and breath / panting vapor / transcutaneous vapor (fractionated relative to body water). The Kohn model, converted to the form of isotope ratios and fractionation factors, is given by:

$$\sum f_i \cdot \alpha_{i-\mathrm{mw}} \cdot R_{\mathrm{mw}} + f_{\mathrm{O_2}} \cdot \alpha_{\mathrm{in-O_2}} R_{\mathrm{O_2}} = \sum f_o \cdot \alpha_{o-\mathrm{bw}} \cdot R_{\mathrm{bw}} \quad (18)$$

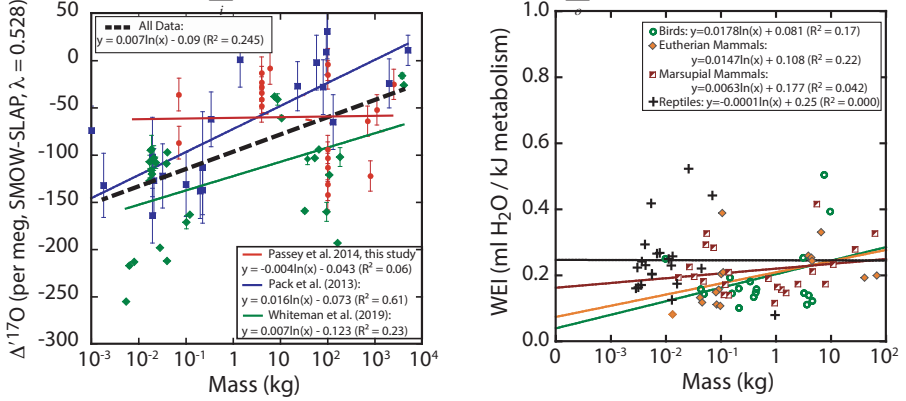

Figure 8. Mammal and bird body water $\Delta'^{17}O$ values and water economy index (WEI) as a function of body mass. **A.** Body water $\Delta'^{17}O$ versus body mass. **Squares** are data from Pack et al. (2013), **circles** from Passey et al. (2014), and **diamonds** from Whiteman et al. (2019). The apatite phosphate data from Pack et al. (2013) were converted to the $\lambda = 0.528$ reference frame, and equivalent body water compositions were calculated using $^{18/16}\alpha_{\mathrm{ap\text{-}bw}} = 1.0173$ and $\theta_{\mathrm{ap\text{-}bw}} = 0.523$ (Pack et al. 2013). The apatite carbonate acid-digestion CO_2 data from Passey et al. (2014) were converted to body water using $^{18/16}\alpha_{\mathrm{ap,carb\text{-}bw}} = 1.0332$ and $\theta_{\mathrm{ap,carb\text{-}bw}} = 0.5245$. The eggshell carbonate data from Passey et al. (2014) were converted to body water using $^{18/16}\alpha_{\mathrm{carb\text{-}bw}} = 1.0380$ and $\theta_{\mathrm{carb\text{-}bw}} = 0.5245$ (see Passey et al. 2014; Table 3 footnotes for details). The Whiteman et al. (2019) data were reported as body water, so no conversion was necessary. **B**. WEI versus body mass for birds, eutherian mammals, marsupial mammals, and reptiles. Data are from Nagy and Petersen 1988.

where f_i and f_o are the fractional inputs and outputs of oxygen from each source, $a_{i\text{-}mw}$ are the fractionations of the oxygen inputs relative to meteoric water (R_{mw}), $a_{o\text{–}bw}$ are the fractionations of oxygen outputs relative to body water (R_{bw}), f_{O_2} and R_{O_2} are the fractional contribution and isotopic composition of atmospheric oxygen, and $a_{in\text{–}O_2}$ is the fractionation of oxygen during uptake in the lungs.

Figure 9 shows the different fluxes considered in the Kohn model, and the associated isotopic fractionations. A central aspect of the Kohn model is the use of taxon-specific water economy index values (WEI): this is the water use efficiency of the animal, measured in terms of volume of liquid water per unit metabolic energy (e.g., ml/kJ). In essence, WEI is the water usage "per unit of living" (Nagy and Petersen 1998), and relates to adaptations for water conservation such as the urea-concentrating abilities of the kidneys, the ability of animals to tolerate changes in body temperature (and thus reduce the need for evaporative cooling, an adaptation termed 'adaptive heterothermy'), and the ability to avoid heat (e.g., burrowing).

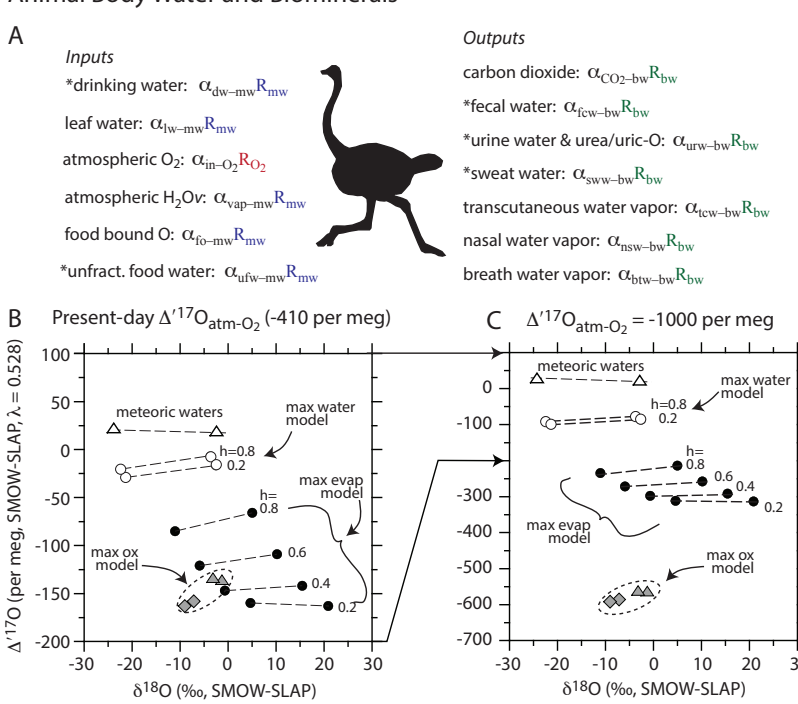

Figure 9. Triple oxygen isotope body water model (Eqn. 18) based on the Kohn (1996) model. **A.** Graphical depiction of the isotopic inputs and outputs considered in the model. For uniformity, all fluxes have an assigned fractionation factor (α), but those marked with an asterisk are unity (i.e., α = 1, no isotopic fractionation). $^{18/16}\alpha$ values are as reported by Kohn (1996), except for leaf water, for which we use a modified version of the Flanagan et al. (1991) model (Roden et al. 2000). θ values are as follows: leaf water: $\theta = -0.008h + 0.522$ (Landais et al. 2006, where h is relative humidity); atmospheric O_2: θ = 0.5179 (Pack et al. 2013; Luz and Barkan 2005); atmospheric water vapor: θ = 0.529 (Barkan and Luz 2005); food bound O: 0.5275 (best guess by Pack et al. 2013; no data are available); carbon dioxide: θ = 0.5248 (Cao and Liu 2011, a theoretical prediction in close agreement with our unpublished experimental value of 0.5243); transcutaneous water: θ = 0.5235 (no data available; this value is intermediate between molecular diffusion of water vapor in air (0.5185) and equilibrium liquid–vapor exchange (0.529); nasal water vapor and breath water vapor: θ = 0.529 (Barkan and Luz 2005). **B.** Evaluation of the model for max water, max evap, and max ox physiologies (see text), modeled with $\Delta'^{17}O(O_2) = -410$ per meg (the value for modern atmosphere measured by Pack et al. 2017). **C.** As (B), but modeled with $\Delta'^{17}O(O_2) = -1000$ per meg, which corresponds to pCO_2 = 940 ppm in the Cao and Bao (2013) model under present-day global gross primary productivity (GPP) and pO_2.

Compilations of WEI for different animals show only weak correlation with body mass (Fig. 8B). Contrary to common expectations, animals with high metabolic rates (and hence high *absolute* rates of O_2 intake) do not consistently have higher *relative* intakes of O_2 compared to other sources of oxygen (e.g., drinking water, plant water). For isotopic mass balance, it is the relative sizes of different fluxes (i.e., fractional contributions) that are important.

The WEI value becomes important in the Kohn model because it determines the amount of liquid drinking water that the animal must consume. The total energy requirement of the animal is determined based on body mass using allometric scaling equations, and this value along with WEI determines the water requirement of the animal. If other sources of water to the animal (plant water, metabolic water) are less than this requirement, then the drinking water influx is used to make up the difference. If other sources of water are in excess of the animal's water requirement, then no drinking water is consumed, and the excess water exits the animal via nonfractionating mechanisms (e.g., urinary and fecal water).

Figure 9 shows predictions of the Kohn model for three endmember animal physiologies. In the 'maximum water' (max water) scenario, the animal is highly dependent on drinking water (WEI = 0.6 ml/kJ), consumes very little leaf water (which is strongly modified by evaporation; see Fig. 12), has relatively low digestibility and high fecal water content (more fecal water means more water loss per unit of energy metabolized) and has non-fractionating water effluxes (e.g., sweat versus panting). The hippopotamus is an example of a 'max water' physiology. In the 'maximum evaporation' (max evap) scenario, the animal obtains most of its water in the form of leaf water, which is strongly modified by evaporation). The animal is extremely water-efficient (WEI = 0.05 ml/kJ) and hence drinks little or no water, has high digestibility and low fecal water content, and loses water via fractionating mechanisms (panting versus sweating). Selective browsers such as giraffe, deer, and ostrich are examples of 'max evap' physiologies. Finally, in the 'max oxygen' (max ox) scenario, the degree of O_2-sourced oxygen is maximized by imparting the animal with low WEI (0.05 ml/kJ), a diet high in fats and low in free watercontent (which increases the fraction of metabolic water and hence usage of O_2), high digestibility, and low fecal water content. Kangaroo rats and other highly-water-independent desert animals are examples of max ox physiologies.

Figure 10 shows the published data in the context of these model predictions. There is general agreement between models and data. For example, highly water-dependent species such as river otters, elephants, hippos, and humans tend to have high $\Delta'^{17}O$ values. Of special interest are domestic birds (Fig. 10B), including ostrich, which is normally a water-independent species. The domestic birds all have high $\Delta'^{17}O$, consistent with a dry pellet diet that necessitates substantial drinking, which ties the triple isotope composition of these animals close to the composition of meteoric waters. Animals known to be selective leaf consumers (browsers) generally have low $\Delta'^{17}O$, reflective of the signature of leaf water; this includes giraffe, deer, and ostrich. Finally, most of the rodents plot in the direction of the max ox and max evap models. The most conspicuous inconsistency between the model predictions and observations is for the desert rodents in the dataset of Whiteman et al. (2019): many of these data are 50 to 100 per meg lower in $\Delta'^{17}O$ than predicted by the model! It is unclear at this point why the data / model discrepancy exists. In terms of the modeling, a major uncertainty is the fractionation between atmospheric oxygen and the oxygen that is absorbed by the lungs. It is known that the lungs discriminate against ^{18}O by several per mil (Epstein and Zeiri 1988), with values for free-ranging animals poorly known (Kohn 1996). No measurements of θ values for this process have been made, and if the true value is substantially higher than the estimate by Pack et al. (2013) used here (θ = 0.5179; Luz and Barkan 2005), then modeled body water values would be lower in $\Delta'^{17}O$. Furthermore, there may be aspects of the burrow enviroment of these desert rodents that influence isotopic compositions (i.e., the composition of soil water vapor,

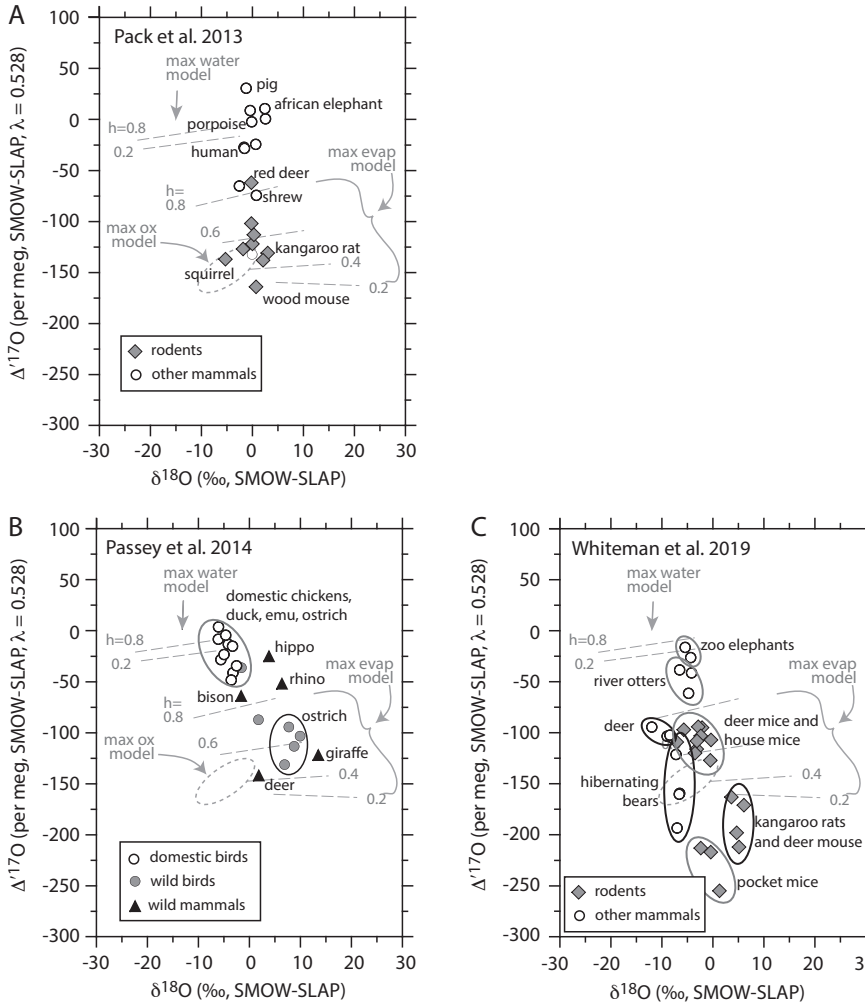

Figure 10. Measured triple oxygen isotope compositions of animals. All datasets are presented in the context of the max water, max evap, and max ox models shown in Figure 9B. **A.** Dataset of Pack et al. (2013). **B.** Dataset of Passey et al. 2014, with the addition of three new data points: a modern giraffe from Tsavo National Park, Kenya ($\delta^{18}O$ = 13.5‰, $\Delta'^{17}O$ = −122 per meg), a modern deer from Parowan, Utah, USA ($\delta^{18}O$ = 1.9‰, $\Delta'^{17}O$ = −142 per meg), and a modern bison from Antelope Island, Utah, USA ($\delta^{18}O$ = −1.6‰, $\Delta'^{17}O$ = −64 per meg). **C.** Dataset of Whiteman et al. (2019). See Figure 8 caption for explanation of how the bioapatite phosphate data of Pack et al. (2013) and the bioapatite carbonate and eggshell carbonate data of Passey et al. (2014) were converted into equivalent body water values.

and even O_2, which may be isotopically fractionated by respiration in soils), and the soil water available to plants (and hence food) may be modified by evaporation. These discrepancies highlight the need for ongoing research both in terms of collecting data from modern animals and environments, determining key fractionation exponents, and refining models.

Stepping back, the results presented in Figure 10 are very encouraging for application of triple oxygen isotopes to animals: The observed ranges in $\Delta'^{17}O$ are the largest out of any system discussed in this chapter, and there is clear ecological patterning that makes sense

in the context of the current state of modeling. As yet published datasets developed by our group for modern mammals (Lehmann 2016) and dinosaurs (Hu 2016) point to clear signals of aridity and changes in $\Delta'^{17}O$ of past atmospheric O_2, respectively. A such, studies of triple oxygen isotopes in animals promise to reveal information not only about past climates, but also about paleoecology and past global biogeochemical cycles.

Prospects for reconstructing $\Delta'^{17}O$ of past atmospheric O_2

The wide variation in $\Delta'^{17}O$ of extant animals—and therefore certainly for extinct animals as well—may appear to portend badly for the prospects of precisely reconstructing $\Delta'^{17}O$ of past atmospheric O_2 based on analyses of fossil teeth, bones, and eggshell. However, this variability can potentially be embraced and used to good effect towards reconstructing both $\Delta'^{17}O(O_2)$ and aspects of paleoecology and paleoclimate. As Figure 9B predicts, animal communities living in times of high pCO_2 and hence anomalously-low $\Delta'^{17}O(O_2)$ (here, −1000 per meg) will be shifted downwards in $\Delta'^{17}O$ and will have a greater range in $\Delta'^{17}O$. Therefore, in an approach where data are generated for specimens from multiple taxa, the utility of the $\Delta'^{17}O(O_2)$ signal lies not in the absolute value of any particular specimen, but in the $\Delta'^{17}O$ values of the upper and lower limits of the population (i.e., position and range in $\Delta'^{17}O$ space). Figure 11 shows the max water, max evap, and max ox models calculated as a function of $\Delta'^{17}O(O_2)$, evaluated for a relative humidity of 0.2 (i.e., an extreme low limit). Figure 11 also shows the highest 10 and lowest 10 $\Delta'^{17}O$ values observed for modern animals, plotted as horizontal bars, corresponding on the vertical axis to the observed $\Delta'^{17}O$ value of each sample, and on the *x*-axis to range in $\Delta'^{17}O(O_2)$ that is permissible for the sample. Note that this approach requires no information about the water balance physiology of specific animals. For the community as a whole, there should be a limited, concordant range in $\Delta'^{17}O(O_2)$ values that can explain all of the data. We term this the environmental physiology isotope concordance (EPIC) approach (Hu 2016): If the body water endmember models are appropriate for extinct organisms, and if all animals analyzed in an assemblage existed under a uniform value of $\Delta'^{17}O(O_2)$, and if diagenesis is not a factor, then there should be a concordant range in $\Delta'^{17}O(O_2)$ values that can explain all of the data.

Clearly, reliable implementation of this EPIC approach will be a challenging task. It will require highly-vetted body water models that reliably bracket the range of common water balance physiologies for terrestrial animals. The data in Figure 8B suggests that this may be tractable: water economy relative to metabolic demand for O_2 falls within fairly narrow limits, for the vast majority of organisms, with no systematic differences among reptiles, birds, marsupial mammals, and eutherian mammals. Given that the present-day manifestation of the extant range of water balance physiologies is the product of more than 400 million years of evolution of separate lineages animals on the continents, it is probably safe to assume that ranges were not hugely dissimilar during e.g., the reign of the dinosaurs in the Mesozoic, or during radiation of mammals in the Cenozoic. The EPIC approach will require the analysis of a wide range of species that existed more or less at the same time (from contemporaneous fossil assemblages), which is challenging both in terms of finding suitable assemblages, and in the laboratory challenge of analyzing often very small fossils that make up the majority of the diversity (e.g., rodents, early mammals, dinosaur teeth with extremely thin tooth enamel). Diagenesis will need to be addressed through both microanalytical methods and stable isotope approaches. All of these challenges are considerable, but the scientific products—records of pCO_2, paleoecology of extinct species, and paleoclimate—are also considerable, and will make the effort worthwhile.

Plant waters

Actively transpiring leaves are evaporatively-enriched in ^{18}O (Gonfiantini et al. 1965), whereas there is no measurable fractionation during soil water uptake by the roots, nor during transport in the xylem (White 1989; Ehleringer and Dawson 1992). Although more recent

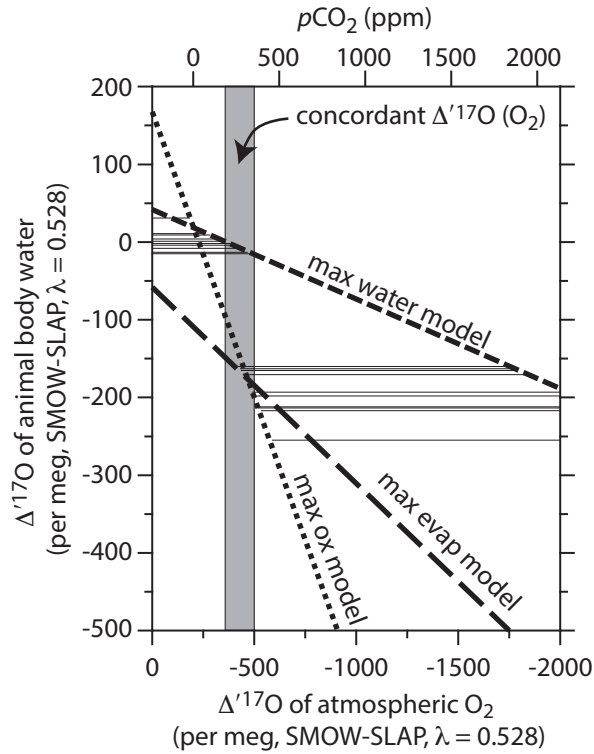

Figure 11. Illustration of the environmental physiology isotopic concordance (EPIC) approach for determining the $\Delta'^{17}O$ of atmospheric O_2 ($\Delta'^{17}O(O_2)$) based on triple oxygen isotope analysis of vertebrate biogenic carbonates. **Bold dashed lines** show the max water, max evap, and max ox body water models evaluated as a function of $\Delta'^{17}O(O_2)$. **Thin horizontal lines** mark the $\Delta'^{17}O$ values (*y*-axis) of the highest 10 and lowest 10 observed values in the combined datasets of Pack et al. (2013), Passey et al. (2014), and Whiteman et al. (2019). The horizontal extent of each line is bounded by the intersections with the body water model lines. In other words, the extent of each horizontal line shows the range of $\Delta'^{17}O(O_2)$ values that could give rise to the measured body water $\Delta'^{17}O$ value. Omitted for clarity are horizontal lines for the 76 additional samples that fall between the highest 10 and lowest 10. The **gray field** shows the range of $\Delta'^{17}O(O_2)$ values that are concordant with all of the observed 96 data points, excluding the highest five and lowest five values as a measure of outlier removal. The resulting field overlaps the present-day $\Delta'^{17}O(O_2)$ of –430 per meg, and is consistent with the pre-industrial CO_2 level of 280 ppm. Note that because the residence time of atmospheric O_2 is of order 10^3 years, the $\Delta'^{17}O(O_2)$ value has not changed substantially during the past 150 years, and therefore reflects an atmosphere with ~280 ppm CO_2. The relationship between pCO_2 (top axis) and $\Delta'^{17}O(O_2)$ is from the model of Cao and Bao (2013).

and detailed models exist (see the review by Cernusak et al. 2016), the leaf water evaporation model presented by Flanagan et al. (1991) is a straightforward steady-state model based on the Craig–Gordon evaporation model, and a good entry point for understanding isotopic enrichment in leaves:

$$R_{\text{leaf}} = \alpha_{\text{eq}}\left[\alpha_{\text{k}}R_{\text{s}}\left(\frac{e_{\text{i}}-e_{\text{s}}}{e_{\text{i}}}\right)+\alpha_{\text{kb}}R_{\text{s}}\left(\frac{e_{\text{s}}-e_{\text{a}}}{e_{\text{i}}}\right)+R_{\text{a}}\left(\frac{e_{\text{a}}}{e_{\text{i}}}\right)\right] \tag{19}$$

where R_{leaf}, R_{s}, and R_{a} are the isotope ratios of leaf water, soil water, and atmospheric water vapor, respectively, α_{k} is the fraction factor for molecular diffusion of water vapor in air, a_{kb} is the effective fractionation factor for water vapor transport through the boundary layer adjacent to the

leaf surface (analogous to α_{diff}), and e_i, e_s, and e_a are the water vapor pressures in the intercellular air spaces inside the leaf, at surface of the leaf, and in the free atmosphere, respectively. For adaptation to ^{17}O, the following θ values are used: $\theta_k = \theta_{kb} = 0.5185$, $\theta_{eq} = 0.529$.

Figure 12 shows the predictions of this model for a range of relative humidities, along with measured values for leaves, stems/roots, and soil water presented by Landais et al. (2006; for plants from Israel and some locations in Europe) and Li et al. (2017; for plants from Kenya). We omit growth-chamber data from Alexandre et al. (2018), which show similar trends. Why do leaf waters have such low $\Delta'^{17}O$ values compared to e.g., evaporating pans of water and closed-basin lakes? The answer lies in the stagnant environment of the intercellular air spaces inside of the leaf, which allows for full expression of the isotope fractionation associated with molecular diffusion of water vapor down the concentration gradient from 100% rh inside of the leaf to <100% rh at the leaf surface. This fractionation is not fully expressed during evaporation from open water surfaces (such as lakes) owing to turbulence.

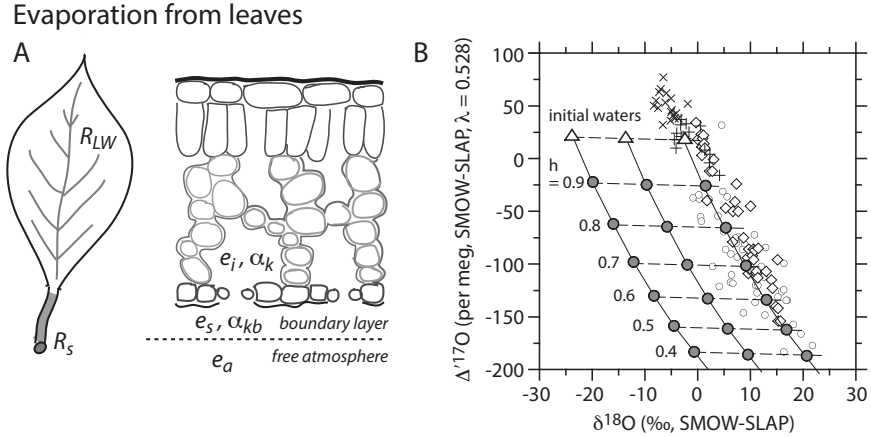

Figure 12. Triple oxygen isotope compositions of leaf waters. **A.** Schematic diagram showing the intercellular, boundary layer, and free atmosphere regions considered in the leaf water model (Eqn. 19). **B.** Modeled steady-state compositions of leaf water, modeled as a function of relative humidity. **Gray circles** show steady state compositions for the indicated relative humidities and source waters (i.e., stem waters) indicated by the **triangles**. **Small crosses** and **open circles** show stem water and leaf water data from Landais et al. (2006). **Small plus signs** and **open diamonds** show stem and leaf water data from Li et al. (2017).

The fact that leaf water has distinctive $\Delta'^{17}O$ is not only of consequence for leaves or the animals that eat them. Leaf water influences the isotopic composition of atmospheric CO_2 and O_2, so a thorough understanding of global leaf water triple oxygen isotope compositions will be essential for understanding the triple oxygen isotope global biogeochemistry of these species (Liang et al. 2017). The isotopic composition of plant macromolecules such as cellulose, of which tree rings are largely composed, are strongly influenced by the leaf water (Roden et al. 2000), meaning that there should be signals of past climate (e.g., relative humidity) preserved in $\Delta'^{17}O$ of tree rings. Phytoliths preserve lasting records of plant ecophysiology, and the triple oxygen isotope composition of these correlates strongly with relative humidity (Alexandre et al. 2018). Much important research into the triple oxygen isotope systematics of plants remains to be done, given that only three detailed studies have been published so far (Landais et al. 2006; Li et al. 2017; Alexandre et al. 2018).

ANALYSIS OF CARBONATES AND BIOAPATITES

The modern era of triple oxygen isotope hydroclimate begins with Barkan and Luz (2005), who improved the water CoF_3 fluorination methods of Baker et al. (2002) to achieve precisions in $\Delta'^{17}O$ of better than 10 per meg. Laser-based methods are increasingly employed to analyze waters, although not always with a substantial savings in time or effort, given the intensive sample – standard bracketing that is necessary to achieve accuracy and precision at the 10 per meg level (Berman et al. 2013; Steig et al. 2014; Tian et al. 2018).

The high-precision analysis of carbonates has been hampered by the fact that carbon dioxide released by phosphoric acid digestion contains ^{13}C. This means that carbon dioxide of nominal mass 45 consists both of $^{13}C^{16}O_2$ (44.9932 u), and $^{12}C^{17}O^{16}O$ (44.9940 u). The mass difference between these isotopologues is 0.0008 u, which is well under the mass resolving power of typical isotope ratio mass spectrometers, and is even beyond the capabilities of the Thermo 253 Ultra and Nu Panorama instruments. Therefore, the O in carbonate minerals or CO_2 derived from acid digestion of those minerals needs to be converted to, or equilibrated with, a gas that has no interfering isobars for the ^{17}O-containing isotopologues. This gas is molecular oxygen, where $^{17}O^{16}O$ has a mass of 32.9940 u. In general, the approaches that have been developed can be categorized as 'conversion methods', where nominally all of the O in $CaCO_3$ (or CO_2) are converted to O_2, or 'exchange methods', where CO_2 is exchanged with subequal quantities of O_2 or another phase (H_2O, CeO_2) that can be more easily fluorinated to produce O_2, or where CO_2 is analyzed before and after exchange with a large, uniform oxygen reservoir of known isotopic composition, which permits back-calculation of the $\delta^{17}O$ of CO_2. A third emerging category bypasses the problem altogether by performing mass spectrometry on O^+ ion fragments from electron impact with CO_2 (Adnew et al. 2019), or by using laser spectroscopy (Sakai et al. 2017).

All of the methods achieving high precision (~10 per meg or better for $\Delta'^{17}O$) employ extended collection time dual inlet mass spectrometry. Ion currents are typically in the range of a few tens of nA for the major *m/z* 32^+ ion beam, and collection times are commonly ~1000–2000 s, distributed over several tens of sample gas / reference gas cycles. *m/z* 33 is typically registered through ~10^{11} to ~10^{12} Ω resistors. Shot-noise limited precision for $\Delta'^{17}O$ under such analytical conditions is on the order of 5 per meg, as calculated using Merritt and Hayes (1994, Eqn. 15).

Conversion methods

Direct fluorination. Compared to other methods discussed here, there is a fairly long history of directly fluorinating carbonate minerals and carbon dioxide to produce O_2 for mass spectrometry (Sharma and Clayton 1965; Miller et al. 2002; Benedix et al. 2003). Nevertheless, the analysis has been uncommon, in part because $\delta^{18}O$ could be more readily analyzed by phosphoric acid digestion and analysis of CO_2, and in part because $CaCO_3$ and CO_2 are highly refractory with respect to F_2 / BrF_5, requiring high temperatures (~ > 700 °C) and very long reaction times (~4 days) for quantitative conversion to O_2. Wostbrock et al. (2020) have recently revived this method and adapted it for high-precision triple oxygen isotope analysis. A key aspect of their method, and indeed one that is common amongst most of the successful methods achieving high precision in $\Delta'^{17}O$, is the careful post-fluorination clean-up of O_2 using a molecular sieve GC column (e.g., Pack and Herwartz 2014). Following fluorination of $CaCO_3$ or CO_2 for 96 hours at 750 °C, Wostbrock et al. (2020) pass the O_2 gas over two lN_2-temperature traps, through a 100 °C NaCl trap to remove traces of F_2, through an additional lN_2 temperature trap, and then absorb the gas onto a 5Å molecular sieve. The O_2 is then released into a helium stream that carries it through a 6' long, 1/8" diameter molecular sieve gas chromatography column held at room temperature. The O_2 is then recollected on molecular sieve, and finally introduced into the mass spectrometer. All of this clean-up is to ensure that the O_2 gas is free of isobars, including NF_3, which can be fragmented into the *m/z* 33 NF^+ ion in the ion source of the mass spectrometer.

Although the method of Wostbrock et al. (2020) is the 'newest kid on the block' with respect to the modern era of triple oxygen isotope analysis of carbonates, we are of the opinion that their method is currently the best available for accurate and relatively assumption-free determination of $\Delta'^{17}O$ values of carbonates. This is because the method features verifiable 100% conversion of $CaCO_3$ oxygen to O_2 oxygen, and hence there can be no isotope fractionation, barring exchange with O inside of the extraction apparatus, the possibility of which can be monitored using $\delta^{18}O$ values, and mitigated by running several replicates in series. As described below, other methods involve measurable blank and fractionation effects, and oftentimes require bespoke calculations to arrive at the final $\Delta'^{17}O$ value of the carbonate. No such steps are required for the fluorination analysis aside from standardization within the SMOW-SLAP reference frame: the $\Delta'^{17}O$ of the O_2 gas measured by the mass spectrometer *is* the $\Delta'^{17}O$ of the $CaCO_3$ (or CO_2), with no calculations or corrections required. Additionally, water (including VSMOW and SLAP) are analyzed on the same extraction line using nearly identical procedures, and furthermore the silicate oxygen isotope scale is calibrated using the same methods. For these reasons, we suggest that direct fluorination, when conducted properly, be considered as the 'gold standard' method that is used to standardize the $\Delta'^{17}O$ values of carbonate minerals in the VSMOW-SLAP reference frame. These standardized $\Delta'^{17}O$ values can then be used to normalize data from other methods into a common reference frame.

Direct laser fluorination is used by Gehler et al. (2011, 2016) and Pack et al. (2013) to analyze the phosphate component of bioapatite (primarily tooth enamel). The methods are similar to those developed for laser fluorination of silicates, except that the bioapatite sample is first fused under argon at 1000 °C to drive off organic matter and oxygen from the carbonate and hydroxide components of bioapatite.

Acid digestion–reduction–fluorination. Passey et al. (2014) developed a method similar to that conceived by Brenninkmeijer and Röckmann (1998), whereby carbon dioxide generated by phosphoric acid digestion of carbonate or bioapatite is reduced in the presence of excess molecular hydrogen and Fe catalyst to produce H_2O, with the carbon exiting as methane. The water is then fluorinated over CoF_3 to produce O_2, largely following the methods of Barkan and Luz (2005). The sluggish reaction kinetics of the reduction reaction ($CO_2 + 4H_2 \rightarrow CH_4 + 2H_2O$) are addressed by using a closed circulating loop reactor design, which ensures that unreacted CO_2 can pass through the reactor multiple times for complete conversion to $CH_4 + H_2O$. The reaction takes place at 560 °C inside of a glassy carbon tube, which is essential to minimize exchange with O that might occur inside of a fused silica reactor, and to avoid unwanted catalytic activity and exchange with oxides that might occur inside of an iron- or nickel- based reactor tube. Observations using a Thermo ISQ7000 quadrupole mass spectrometer in our laboratory at Michigan have verified that CO is an intermediate product of the reaction. During several passes through the reactor, the CO is converted to $CH_4 + H_2O$. It also appears likely that C is deposited onto the Fe catalyst, and subsequently reduced to CH_4 by reaction with the excess H_2. At any rate, the product of interest in the reaction is H_2O, which is trapped from the circulating loop at −78 °C (dry ice temperature), and is then purged through a CoF_3 reactor via a helium stream, according to the basic procedures of Barkan and Luz (2005). The produced O_2 is cleaned-up by passage through a multi-loop open nickel tube immersed in liquid nitrogen (to remove HF produced in the fluorination reaction), and then through a ~1.2 m, 1/8" o.d. 5Å molecular sieve GC held at −78 °C. The O_2 leaving the GC is trapped onto a 5Å molecular sieve held at liquid-N_2 temperature, then expanded at 90 °C for 10 minutes, and finally admitted into the mass spectrometer.

The precision for this analysis is ~10 per meg. The method achieves nominally 100% yield, but has clear exchange and fractionation effects, which are revealed by comparing known $\delta^{18}O$ values of the carbonates (measured as CO_2) to the $\delta^{18}O$ of O_2 generated by the method (Passey et al. 2014). Slopes of this regression over a range of ~30‰ in $\delta^{18}O$ are typically ~0.95, meaning that the exchange effect is about 5%. Fractionation effects result in mediocre precision in $\delta^{17}O$

and $\delta^{18}O$ values (~0.2‰ and 0.4‰ 1σ, respectively), but these errors are correlated and mass-dependent with a slope near 0.528, which means that $\Delta'^{17}O$ values are virtually unaffected. In our new system at Michigan, we have observed drift in $\Delta'^{17}O$ values within some of our analytical sessions. This drift can have a magnitude of ~10–30 per meg, and is systematic across the ~ 4–5 different carbonate reference materials (NBS−18, NBS−19 / IAEA 603, and some in-house standards) that we regularly analyze throughout our sessions. Therefore, the drift is correctable by normalizing to long-term mean values for our standards (or, ideally in the future, to community consensus $\Delta'^{17}O$ values for standards such as NBS−18 and IAEA 603), in the manner that is common for e.g., continuous flow methods. Because of the blank, fractionation, and drift effects, the method is less appropriate than direct fluorination for defining absolute $\Delta'^{17}O$ values. Merits of the method are that it is relatively safe, that the entire procedure takes only ~2.5 hours per sample (i.e., from dropping the sample in phosphoric acid to admitting the final O_2 product in the mass spectrometer), and, compared to exchange methods, that it requires only one kind of mass spectrometric determination (i.e., analysis of sample O_2).

Exchange methods

Several methods have been developed based on isotopic exchange between CO_2 and another phase that is more amenable to analysis. These include analyzing CO_2 before and after exchange with excess CeO_2 or CuO with known oxygen isotopic composition, which permits back-calculation of the $\Delta'^{17}O$ of the CO_2 (Assonov and Brenninkmeijer 2001; Kawagucci et al. 2005; Mahata et al. 2012; Mrozek et al. 2015), exchange of an excess of CO_2 with CeO_2, which is then fluorinated to produce O_2 (Hoffman and Pack 2010), exchange of subequal amounts of CO_2 and H_2O, fluorination of the H_2O to produce O_2, and back-calculation of the CO_2 composition (Barkan and Luz 2012), and Pt-catalyzed exchange between subequal amounts CO_2 and O_2, analysis of the O_2, and back-calculation of the CO_2 composition (Mahata et al. 2013, 2016). Of these methods, only the latter has become widely-adopted for high-precision analysis (e.g., Barkan et al. 2015, 2019; Liang et al. 2017; Prasanna et al. 2016; Sha et al. 2020; Fosu et al. 2020; Bergel et al. 2020; Voarintsoa et al. 2020), so we will focus our discussion on this method.

Pt-catalyzed CO_2–O_2 exchange. In this method, subequal quantities of CO_2 and O_2 are exchanged over a hot platinum wire or sponge (~750 °C) for ~ 1 h. The isotopic compositions of both gases are analyzed before the exchange. Following the exchange, the CO_2 and O_2 are separated, collected, and reanalyzed separately (either using two mass spectrometers, or by analyzing them in series after switching the configuration of a single mass spectrometer). The $\delta^{17}O$ value of the CO_2 can then be calculated according to (Barkan and Luz 2015):

$$\delta^{17}O_{in}\left(CO_2\right)=\frac{1}{\beta}\left[\left(\delta^{17}O_f\left(O_2\right)+1\right)\left(1+{}^{17}\alpha_{Pt}\cdot\beta\right)-\left(\delta^{17}O_{in}\left(O_2\right)+1\right)\right]-1 \tag{20}$$

where

$$\beta=\frac{\delta^{18}O_{in}\left(O_2\right)-\delta^{18}O_f\left(O_2\right)}{\delta^{18}O_f\left(CO_2\right)-\delta^{18}O_{in}\left(CO_2\right)} \tag{21}$$

and where $\delta^{18}O_f(CO_2)$ can be calculated as:

$$\delta^{18}O_f\left(CO_2\right)={}^{18}\alpha_{Pt}\left(\delta^{18}O_f\left(O_2\right)+1\right) \tag{22}$$

In Equations (20–22), the subscript 'in' refers to the initial (pre-equilibration) isotopic composition, the subscript 'f' refers to the final (post-equilibration) composition, and ${}^{17/16}\alpha_{Pt}$ and ${}^{18/16}\alpha_{Pt}$ are the isotopic fractionations between CO_2 and O_2 when the exchange reaction has reached steady-state.

Of key importance for this method are knowledge of $^{17/16}\alpha_{Pt}$ and $^{18/16}\alpha_{Pt}$ values, and awareness of potential variation in these values. The $^{18/16}\alpha_{Pt}$ and θ_{Pt} values [where $\theta_{Pt} = \ln(^{17/16}\alpha_{Pt})/\ln(^{18/16}\alpha_{Pt})$] values can only be determined using pairs of CO_2 and O_2 with known $\Delta^{17}O$. This presents a challenge, because the $\Delta'^{17}O$ of CO_2 cannot be measured directly, which is the reason for the development of these methods in the first place. In most laboratories, this problem has been addressed by reacting O_2 with known $\Delta'^{17}O$ over hot graphite wound with Pt wire to produce CO_2 (Barkan and Luz 1996). Here it is assumed that if there is no exchangeable oxygen in the system, and if 100% of the O_2 is converted to CO_2, then the $\Delta'^{17}O$ value of the product CO_2 must be the same as that of the O_2. This assumption can be evaluated by measuring the $\delta^{18}O$ of the CO_2 and comparing this to the $\delta^{18}O$ of the O_2 (they should be identical), but it cannot be strictly evaluated in the case of $\delta^{17}O$.

Based on results from different laboratories, there is no single set of $^{18/16}\alpha_{Pt}$ and θ_{Pt} values that characterize the exchange reaction. $^{18/16}\alpha_{Pt}$ values are typically 0.998–1.002 (i.e., ± ~2 per mil or smaller $\delta^{18}O$ difference between exchanged CO_2 and O_2), and θ_{Pt} values are typically ~0.55–0.62. These θ values are well beyond the theoretical high-temperature limit for mass dependent fractionation (0.5305; Young et al. 2002), implying kinetic fraction during the exchange reaction. $^{18/16}a_{Pt}$ and θ_{Pt} values apparently depend on the precise physical configuration of the exchange reactor, and must be determined for each system (Fosu et al. 2020).

These findings underscore the need for (1) agreed upon $\Delta'^{17}O$ values for widely-available carbonate standards that can be used to develop $^{18/16}\alpha_{Pt}$ and θ_{Pt} values for each system, thus obviating the need for each laboratory to develop its own CO_2 gas of 'known' $\Delta'^{17}O$ based on combustion of O_2, given potential errors in this approach, and (2) the routine analysis of (ideally) carbonate standards with known $\Delta'^{17}O$ to monitor for systematic changes in in analytical results. Of course, (2) applies for any analytical method, whereas (1) is uniquely necessary to exchange methods that depend on accurate knowledge of exchange fractionation factors. We suggest that the $\Delta'^{17}O$ values for NBS−19, NBS−18, and IAEA 603 reported by Wostbrock et al. (2020) be provisionally used for these purposes, as these values were determined by the direct fluorination method and normalized to analyses of VSMOW2-SLAP made using the same analytical procedures and equipment. These calibration issues notwithstanding, it appears that several different laboratories are able to produce internally consistent data with high precision, and are able to resolve clear environmental signals when analyzing natural materials (e.g., Liang et al. 2017; Sha et al. 2020; Bergel et al. 2020; Voarintsoa et al. 2020; Fosu et al. 2020).

Other methods

Adnew et al. (2019) explored the measurement of O^+ ion fragments produced from electron bombardment of CO_2 in the ion source of the Thermo 253 Ultra mass spectrometer. The benefit of such a method is the ability to measure CO_2 directly, sidestepping the need for lengthy chemical conversion or exchange procedures. Of particular challenge with this method is the relatively inefficient production of these ions, and the interferences of $^{16}OH^+$ and $^{16}OH_2^+$ on the $^{17}O^+$ and $^{18}O^+$ signals, respectively. The high mass resolving power of the 253 Ultra, however, permits clear resolution of these ions on the low-mass shoulders of the larger $^{16}OH^+$ and $^{16}OH_2^+$ peaks. Precisions for $\Delta'^{17}O$ of 14 ppm (SEM) can be achieved with counting times of 20 hours.

Tunable Infrared Laser Direct Absorption Spectroscopy (TILDAS) shows great promise for high precision analysis of $\Delta'^{17}O$ in CO_2 (Sakai et al. 2017; Prokhorov et al. 2019). In the region of wavenumber 2310 cm^{-1}, the four most abundant isotopologues of CO_2 are clearly resolved, with only minor overlap between $^{12}C^{17}O^{16}O$ at 2309.98 cm^{-1}, and $^{12}C^{16}O_2$ at 2310.00 cm^{-1}. Sakai et al. (2017) report standard errors of less than 0.04‰ and 0.03‰ for $^{18}O/^{16}O$ and $^{17}O/^{16}O$, respectively, on CO_2 released from sub-100 µg $CaCO_3$ samples (i.e., about 50× less material than is required for most of the methods described above). Both Sakai et al. (2017) and Prokhorov et al. (2019) show tight correlations between $\delta^{17}O$ and $\delta^{18}O$ measured for

suites of samples spanning a large range in isotopic composition. These papers stop short of presenting $\Delta'^{17}O$ values. However, Wang et al. 2020, achieved precisions of 10 per meg on the $^{13}C^{18}O^{16}O$ 'clumped' isotopologue using a similar instrument from the same manufacturer as the TILDAS used in Sakai et al. (2017; Aerodyne Research, Inc.). Given that this isotopologue is 16 times less abundant than $^{12}C^{17}O^{16}O$, it seems likely that TILDAS will eventually achieve the 10 per meg precision benchmark for $\Delta'^{17}O$.

Interlaboratory reproducibility

Several labs have reported $\Delta'^{17}O$ values for the carbonate reference materials NBS18, NBS19, and IAEA 603 (Table 1). Most groups report values for CO_2 released from acid digestion of these materials at 25 °C, while the Johns Hopkins / Michigan labs report values for 90 °C acid digestion, and Wostbrock et al. (2020) report values for the both the carbonate mineral and for the CO_2 liberated by 25 °C acid digestion. For calculation of the equivalent $CaCO_3$ composition from CO_2 values, we use the θ_{acid} value of 0.5230 determined by Wostbrock et al. (2020). This value was determined for 25 °C acid digestion. Guo et al. (2009) predict very little temperature dependence in θ_{acid} (0.00003) between 25 °C and 90 °C, so we provisionally use Wostbrock's value for 90 °C acid digestion data given a lack of θ_{acid} values at this temperature. In Table 1, we present new data from the Michigan lab for all of the carbonate standards that have been analyzed since the measurement was established in May 2008, uncorrected for the intra-session drift noted above. Note that the Michigan lab is effectively a 'different' lab compared to the Johns Hopkins lab (Passey et al. 2014, Passey and Ji 2019), given that the extraction line and mass spectrometer are different.

Table 1 shows that there is very close agreement in $\Delta'^{17}O(CaCO_3)$ values amongst the labs using conversion methods, with standard deviations of 5 per meg or less for the populations of $\Delta'^{17}O$ values for each material. Part of this agreement could be fortuitous given our lack of knowledge of θ_{acid} at 90 °C. Alternatively, it is possible that θ_{acid} has very little temperature sensitivity, as predicted by Guo et al. (2009), in which case the interlaboratory agreement is real. Another measure of methodological agreement is the magnitude of $\Delta'^{17}O$ difference between different materials. The final column in Table 1 shows the difference in $\Delta'^{17}O$ between NBS18 and NBS19. The magnitude of this difference (~50 per meg) is essentially the same across the three labs from which conversion data are reported, with the value from Passey et al. (2014; 37 per meg) showing the most departure from the mean. This agreement lends confidence to these methods.

The results from the exchange methods are more variable. Barkan et al. (2019) attributed part of the difference in their values compared to those reported in Barkan et al. (2015) to the possibility of inhomogeneity between different bottles of reference material. The Sha et al. (2020) values appear to be systematically shifted downward, but the difference between NBS18 and IAEA 603 (which is identical within error to NBS19) is 42 per meg, which is similar to the values derived by conversion methods and the value reported by Fosu et al. (2020). The values of Fosu et al. (2020) are within 20 per meg of the values reported by Wostbrock et al. (2020). Note that Fosu et al. (2020) also used NBS18-CO_2 and NBS19-CO_2 to derive $^{18/16}a_{Pt}$ and θ_{Pt} values, although the $\Delta'^{17}O$ values they report for NBS18 and NBS19 are independent of those determinations. Fosu et al. (2020) to-date have presented the most thorough exploration of variation in $^{18/16}a_{Pt}$ and θ_{Pt} in a single extraction line.

Overall, the results in Table 1 are both encouraging and concerning. It is not clear precisely why the considerable lack of agreement exists for the Pt-exchange method, but the variability in $^{18/16}\alpha_{Pt}$ and θ_{Pt} values observed across different laboratories, the exotic absolute values of θ_{Pt}, and the fact that $^{18/16}\alpha_{Pt}$ values deviate from the value expected for CO_2–O_2 equilibrium at 700–800 °C by several per mil (Fosu et al. 2020), collectively suggest that there are important processes at play that are not fully understood, and that uncharacterized variability in these parameters may be a factor. Additionally, these values are generally determined using CO_2 prepared by Pt-catalyzed combustion of graphite with O_2 of known $\Delta'^{17}O$. If unusual isotope

Table 1. Interlaboratory reproducibility for $\Delta'^{17}O$ of carbonate reference materials.

Source	NBS19		NBS18		IAEA 603		$\Delta\Delta'^{17}O$
	$\Delta'^{17}O$ CO_2	$\Delta'^{17}O$ $CaCO_3$	$\Delta'^{17}O$ CO_2	$\Delta'^{17}O$ $CaCO_3$	$\Delta'^{17}O$ CO_2	$\Delta'^{17}O$ $CaCO_3$	NBS18 – NBS19
Conversion Methods							
Passey et al. (2014)[a]	−135	−95	−98	−58	–	–	37
Passey and Ji (2019)[a]	−143	−103	−88	−48	–	–	55
Wostbrock et al. (2020)[b]	−155	−102	−100	−48	−147	−100	54
Michigan IsoPaleoLab[a]	−142	−102	−91	−51	−148	−108	51
	Avg.	**−100**	**Avg.**	**−51**	**Avg.**	**−104**	**49**
	Std.	**4**	**Std.**	**5**	**Std.**	**5**	**8**
Exchange Methods							
Barkan et al. (2015)[c]	−227	−176	3	54	–	–	230
Barkan et al. (2019)[c]	−182	−131	−163	−112	−187	−136	19
Sha et al. (2020) [c]	–	–	−225	−174	−267	−216	42[d]
Fosu et al. (2020)[c]	−169	−118	−119	−67	–	–	50
	Avg.	**−141**	**Avg.**	**−75**	**Avg.**	**−176**	**100**
	Std.	**30**	**Std.**	**96**	**Std.**	**57**	**114**

Notes: $\Delta'^{17}O$ values are reported in per meg relative to the VSMOW-SLAP scale, $\lambda = 0.528$. $CaCO_3$ values are calculated based on CO_2 values using $\theta_{acid} = 0.5230$ (Wostbrock et al. 2020), $^{18}\alpha_{acid} = 1.0103$ (25 °C reactions) and $^{18}\alpha_{acid} = 1.00812$ (90 °C reactions; Kim et al. 2007), except for the $CaCO_3$ values for Wostbrock et al. (2020), which are directly measured.

[a]. Reduction of CO_2 produced by 90 °C acid digestion, and CoF_3 fluorination of the resulting water.

[b]. Direct BrF_5 fluorination carbonate, and of CO_2 produced by 25 °C acid digestion.

[c]. Pt-catalyzed exchange with O_2 of CO_2 produced by 25 °C acid digestion.

[d]. $\Delta'^{17}O$ difference between NBS18 and IAEA 603.

effects characterize this reaction in the same way they have been demonstrated to characterize the Pt-catalyzed CO_2–O_2 exchange reaction, then the $\Delta'^{17}O$ values of the produced CO_2 may deviate from those of the combustion O_2. For all of these reasons, a logical first step would be to use NBS18-CO_2, NBS19-CO_2, and IAEA 603-CO_2 (or other materials calibrated by direct fluorination methods) to develop or validate $^{18/16}\alpha_{Pt}$ and θ_{Pt} values (e.g., Fosu et al. 2020).

Fractionation exponents for carbonate–water equilibrium, and acid digestion

Calculation of the triple oxygen isotope composition of carbonate and apatite parent waters requires knowledge of the fractionation exponents for mineral–water equilibrium, and for acid digestion. Theoretical predictions by Cao and Liu (2011) for θ_{cc-H_2O} are 0.5235 at 25 °C, and they predict weak temperature dependence over the range 0–100 °C (0.5233–0.5239). More recently, Hayles et al. (2018) calculated a value of 0.5257 at 25 °C, and, Guo and Zhou (2019a) predicted values of 0.5253 to 0.5263 over the 0–100 °C temperature range, with a value of 0.5256 at 25 °C.

Using an empirical approach and the reduction–fluorination conversion method, Passey et al. (2014) reported a value of $\theta = 0.5245$ for combined mineral–water fractionation and acid digestion (90 °C). This value is based on analysis of fresh avian eggshell carbonate and water extracted from the same eggs (egg whites), and from analysis of an estuarine oyster and a marine coral and the waters they were found in at the time of sampling. Unpublished data from slow calcite precipitations in our laboratory (passive degassing) over a temperature range of 0–60 °C give a mean value of $\theta = 0.5242$ for combined mineral–water fractionation and acid

digestion, with no resolvable relationship with temperature. More recently, Sha et al. (2020) studied cave dripwater / speleothem pairs and obtained a value of 0.5235 combined mineral–water fractionation and acid digestion at 25 °C using the Pt-exchange method. Bergel et al. (2020) used the Pt-exchange method to derive a value of $\theta = 0.5231$ for combined mineral–water fractionation and acid digestion at 25 °C, based on analyses of freshwater mollusks from well-constrained spring environments. Voarintsoa et al. (2020) of the same laboratory observed a value of $\theta = 0.5225$ for laboratory-precipitated carbonates in the temperature range 10 to 35 °C. Neither study observed clear temperature dependence of the θ value, although the 35 °C values were distinctly lower ($\theta = 0.5220$), which may reflect disequilibrium during very rapid precipitation of this material. Voarintsoa et al. (2020) observe no clear influence of carbonate polymorph (calcite vs. aragonite) or parent solution concentration on θ values.

The only direct measurement of the θ_{acid} value is that of Wostbrock et al. (2020), who report a value of 0.5230 for 25 °C reactions, which is substantially lower than an early theoretical prediction of 0.5283 by Guo et al. (2009).

The variability in θ values described above probably arises from a combination of methodological differences, differences in the exact nature of the θ value (i.e., mineral–water, or acid-digestion-produced CO_2–water, with two different acid digestion temperatures used). Even if more reliable experimental estimates are obtained (i.e., from direct fluorination of laboratory-precipitated carbonates), it may still be the case that each laboratory would be better to use its own laboratory-derived θ values, given that these are influenced by the same analytical artifacts as samples processed in those laboratories.

FUTURE DIRECTIONS AND CONCLUDING REMARKS

We have summarized the considerable progress that has been made during the past 15 years in the exploration and application of triple oxygen isotopes to continental hydroclimate, and have hopefully imbued the reader with an appreciation of the great potential for using triple oxygen isotopes in mineral records to unravel aspects of past climate and ecology. Despite the progress that has been made, the number of detailed studies into many systems such as lakes, plants, and animals can still be counted on one hand (or maybe two!), and many systems are just beginning to be studied or remain unstudied.

Soil carbonates. Triple oxygen isotope studies of soil carbonates promise to reveal the extent to which soil waters from which the carbonates precipitated were evaporatively enriched in heavy isotopes, as well as changes in the $\Delta'^{17}O$ of precipitation that may result from changes in regional atmospheric moisture sources. To our knowledge, the only published data for soil carbonates are the handful of data points in Passey et al. (2014) for modern soils in Inner Mongolia, California, and Ethiopia. Based on that dataset, and emerging data from our lab (Ji 2016; Emily Beverly, Julia Kelson, and Tyler Huth, pers. comm.), $\Delta'^{17}O$ values for soil carbonate parent waters typically fall somewhere between values typical of meteoric waters, and values typical of closed-basin lakes. In other words, many samples show signs of evaporative modification, but the degree of lowering of $\Delta'^{17}O$ is typically less than that observed for closed basin lakes. As was the case in the study of clumped isotopes in soil carbonates, it is becoming clear that triple oxygen isotopes will tell us as much about the seasonal timing and circumstances of soil carbonate formation as they will about prevailing climatic conditions.

Speleothems. Sha et al. (2020) have presented the first triple oxygen isotope data for speleothems, studying a variety of samples from several caves around the world. Based on the present knowledge of triple oxygen isotope systematics, we can expect that cave drip water triple oxygen isotope compositions will vary with: (1) precipitation compositions, which are sensitive both to the effective relative humidity and turbulence over the oceans during the production of

atmospheric vapor bodies (e.g., Fig. 2), and (2) evaporative modification of precipitation before it infiltrates into the subsurface or, in the case of rh < 1 caves, within the cave environments (Fig. 5). The speleothem mineral will record these factors, as well as (3) any kinetic effects that characterize the mineral growth process. Guo and Zhou (2019a,b) have explored the triple oxygen isotope systematics of the system DIC–H_2O–$CaCO_3$, and have developed a reaction–diffusion model to incorporate their predictions of triple isotope fractionation exponents into the transient process of mineralization. They predict kinetically-driven isotope trajectories with initial slopes of ~0.535, meaning that an array of kinetically-influenced sample would plot with a positive slope on a plot of $\Delta'^{17}O$ ($\lambda = 0.528$) versus $\delta^{18}O$. This is a distinctive slope compared to the universally negative slopes for the different systems that we have described in this review. All of the expected effects for $\Delta'^{17}O$ in speleothems (moisture source effect, evaporation effect, kinetic effect) are subtle (Sha et al. 2020; Tyler Huth, pers. comm.), ranging by a few tens of per meg at most, so improving analytical precision beyond the 10 per meg level will be expedient.

Tree rings and other organics. As far as we are aware, triple oxygen isotopes have not been measured to high precision in organic molecules. This should be possible using direct fluorination or high-temperature reduction to produce CO that could then be reduced to water and fluorinated using the approach of Passey et al. (2014). As shown in Figure 12, leaf water $\Delta'^{17}O$ shows high sensitivity to relative humidity. Plant cellulose derives ~40% (Roden et al. 2000) of its oxygen from xylem water (which is not fractionated relative to soil water), meaning that the evaporation signal will be damped, but that it will still be highly resolvable. Thus, application to tree-ring records could help disentangle variations in $\delta^{18}O$ that are caused by changes in the isotopic composition of precipitation, from those that are caused by changes in evaporative enrichment. Biosynthesis of organic molecules involves isotopic fractionation, the mechanisms of which could possibly be probed using triple oxygen isotopes. Oxygen-containing molecules formed in waters of respiration should carry some of the anomalous triple oxygen isotope composition of atmospheric oxygen.

As for the more 'well studied' systems (precipitation, lakes, plants, animals), the existing datasets are only a beginning. Most of the precipitation data are based on opportunistic sampling, and only the studies of Tian et al. (2018) and Uechi and Uemura (2019) involve the kind of continuous, systematic sampling that will reveal the mechanisms of e.g., seasonal variation in $\Delta'^{17}O$, and allow for determination of amount-weighted $\Delta'^{17}O$ of precipitation. The $\Delta'^{17}O$ of atmospheric water vapor is a fundamental parameter for evaporation, but only a handful of studies have conducted measurements (Uemura et al. 2010; Landais et al. 2012; Lin et al. 2013; Surma et al. 2021, this volume), and of these only the Surma et al. study is from a non-polar continental setting. Lake systems are tremendously understudied, especially in more humid settings that may be less 'exciting' in terms of large evaporative $\Delta'^{17}O$ signals, but that are nonetheless important for understanding the full scope of the system. Back-calculation of isotopic compositions of unevaporated waters (Passey and Ji 2019) could be improved with more sophisticated methods such as Bayesian analysis (e.g., Bowen et al. 2018). Leaves come in a range of physiologies (i.e., blades of grass, conifer needles, typical hardwood leaves) for which detailed $\delta^{18}O$–δD models have been developed (Cernusak et al. 2016). It will be important to expand these models and observations to triple oxygen isotopes, both in terms of understanding biogeochemical fluxes of O_2 and CO_2 (which are influenced by leaf water), and understanding the compositions of water available to herbivores. Very little of the taxonomic diversity of land vertebrates has been explored (e.g., reptiles, birds), and the work on mammals summarized above is only a starting point. If we are to use triple oxygen isotopes of vertebrate biominerals to reconstruct paleoecology, paleoclimate, and paleo-atmospheric composition, then we will need exhaustive study of modern organisms in relation to their environments and physiologies, and the further development and refinement of body water models.

Finally, improvement in inter-laboratory reproducibility is urgent and imperative. Yeung et al. (2018) show that pressure-baseline corrections or continual referencing to well-defined, isotopically-disparate materials (i.e., VSMOW2 and SLAP2) is necessary for accuracy at the 10 per meg level. In terms of standardization protocols, the field is still in the 'wild west' stage compared to more mature fields with similar analytical challenges. Taking carbonate clumped isotopes as an example, a key paper (Dennis et al. 2011) was published 5 years after the first clumped isotope papers were published, outlining a rigorous protocol for standardization. This protocol involved routine analysis of reference materials spanning a wide range in both bulk isotopic composition ($\delta^{13}C$ and $\delta^{18}O$), *and* in magnitude of the Δ_{47} clumping signal. This protocol was almost universally-adopted, and as a result there is remarkable interlaboratory agreement in the field (e.g., Petersen et al. 2019). The analogous approach for $\Delta'^{17}O$ in carbonates would be to employ a suite of at least three, and preferably four carbonate materials, two of which span a wide range in $\delta^{18}O$ and have fairly high $\Delta'^{17}O$, and one (or two) of which span a similar range in $\delta^{18}O$ and have fairly low $\Delta'^{17}O$. Routine analysis of such materials would allow for monitoring of, correction for, issues of scale compression (in the $\Delta'^{17}O$ space), as well as accuracy.

ACKNOWLEDGEMENTS

First and foremost, we express gratitude to the talented group of students and postdocs with whom we've journeyed into the world of triple oxygen isotopes, including our 'founding' crew at Johns Hopkins University (Shuning Li, Huanting Hu, Haoyuan Ji Sophie Lehmann, Nicole DeLuca, and Jessica Moerman), and those who have carried the torch at Michigan (Ian Winkelstern, Emily Beverly, Drake Yarian, Phoebe Aron, Elise Pelletier, Sarah Katz, Natalie Packard, Joonas Wasiljeff, Tyler Huth, Nick Ellis, and Julia Kelson). We thank Andreas Pack and Ilya Bindeman for giving us the opportunity to write this chapter, and Jordan Wostbrock and an anonymous reviewer for insightful reviews.

REFERENCES

Adnew GA, Hofmann MEG, Paul D, Laskar A, Surma J, Albrecht N, Pack A, Schwieters J, Koren G, Peters W, Röckmann T (2019) Determination of the triple oxygen and carbon isotopic composition of CO_2 from atomic ion fragments formed in the ion source of the 253 Ultra high-resolution isotope ratio mass spectrometer. Rapid Comm Mass Spectrom 33:1363–1380

Alexandre A, Landais A, Vallet-Coulomb C, Piel C, Devidal S, Pauchet S, Sonzogni C, Couapel M, Pasturel M, Cornuault P, Xin J, Mazur J-C, Prié F, Bentaleb I, Webb E, Chalié F, Roy J (2018) The triple oxygen isotope composition of phytoliths as a proxy of continental atmospheric humidity: insights from climate chamber and climate transect calibrations. Biogeosciences 15:3223–3241

Assonov SS, Brenninkmeijer CAM (2001) A new method to determine the ^{17}O isotopic abundance in CO_2 using oxygen isotope exchange with a solid oxide. Rapid Commum Mass Spectrom 15:2426–2437

Ayliffe LK, Chivas AR (1990) Oxygen isotope composition of the bone phosphate of Australian kangaroos: Potential as a paleoenvironmental recorder. Geochim Cosmochim Acta 54:2603–2609

Baker L, Franchi IA, Maynard J, Wright IP, Pilinger CT (2002) A technique for the determination of $^{18}O/^{16}O$ and $^{17}O/^{16}O$ isotopic ratios from small liquid and solid samples. Anal Chem 74:1665–1773

Barkan E, Luz B (1996) Conversion of O_2 into CO_2 for high-precision oxygen isotope measurements. Anal Chem 68:3507–3510

Barkan E, Luz B (2005) High precision measurements of $^{18}O/^{16}O$ and $^{17}O/^{18}O$ ratios in H_2O. Rapid Commun Mass Spectrom 19:3737–3742

Barkan E, Luz B (2007) Diffusivity fractionations of $H_2{}^{16}O/H_2{}^{17}O$ and $H_2{}^{16}O/H_2{}^{18}O$ and their implications for isotope hydrology. Rapid Commun Mass Spectrom 21: 2999– 3005

Barkan E, Luz B (2012) High-precision measurements of $^{17}O/^{16}O$ and $^{18}O/^{16}O$ ratios in CO_2. Rapid Commun Mass Spectrom 26:2733–2738

Barkan E, Musan I, Luz B (2015) High-precision measurements of $\delta^{17}O$ and ^{17}O-excess of NBS–19 and NBS–18. Rapid Commun Mass Spectrom 29:2219–2224

Barkan E, Affek HP, Luz B, Bergel SJ, Voarintsoa NRG, Musan I (2019) Calibration of $\delta^{17}O$ and ^{17}Oexcess values of three international standards: IAEA–603, NBS19 and NBS18. Rapid Commun Mass Spectrom 33:737–740

Bao H, Lyons JR, Zhou C (2008) Triple oxygen isotope evidence for elevated CO_2 levels after a Neoproterozoic glaciation. Nature 453:504–506

Benedix GK, Leshin LA, Farquhar J, Jackson T, Thiemens MH (2003) Carbonates in CM2 chondrites: Constraints on alteration conditions from oxygen isotopic compositions and petrographic observations. Geochim Cosmochim Acta 67:1577–1588

Benson LV, White JWC (1994) Stable isotopes of oxygen and hydrogen in the Truckee River-Pyramid Lake surface-water system. 3. Source of water vapor overlying Pyramid Lake. Limnol Oceanogr 39:1945–1958

Bergel SJ, Barkan E, Stein M, Affek HP (2020) Carbonate $^{17}O_{excess}$ as a paleo-hydrology proxy: Triple oxygen isotope fractionations between H_2O and biogenic aragonite, derived from freshwater mollusks. Geochim Cosmochim Acta, in press

Berman ESF, Levin NE, Landais A, Li S, Owano T (2013) Measurement of $\delta^{18}O$, $\delta^{17}O$, and ^{17}O-excess by off-axis integrated cavity output spectroscopy and isotope ratio mass spectrometry. Anal Chem 85:10392–10398

Blumenthal SA, Levin NE, Brown FH, Brugal JP, Chritz KL, Harris JM, Jelhe GE, Cerling TE (2017) Aridity and hominin environments. PNAS 114:7331–7336

Bony S, Risi C, Vimeux F (2008) Influence of convective processes on the isotopic composition ($\delta^{17}O$, δD) of precipitation and water vapor: 1. Radiative-convective equilibrium and Tropical Ocean-Global Atmosphere-Coupled Ocean-Atmosphere Response Experiment (TOGA-COARE) simulations. J Geophys Res 113:D19305

Bowen GJ, Putman A, Brooks JR, Bowling DR, Oerter EJ, Good SP (2018) Inferring the source of evaporated waters using stable H and O isotopes. Oecologia 187:1025–1039

Brenninkmeijer CAM, Röckmann T (1998) A rapid method for the preparation of O_2 from CO_2 for mass spectrometric measurement of $^{17}O/^{16}O$ ratios. Rapid Comm Mass Spectrom 12:479–483

Brinjikji M, Lyons JR (2021) Mass-independent fractionation of oxygen isotopes in the atmosphere. Rev Mineral Geochem 86:197–216

Bryant JD, Froelich PN (1995) A model of oxygen isotope fractionation in body water of large mammals. Geochim Cosmochim Acta 59:4523–4537

Cao X, Bao H (2013) Dynamic model constraints on oxygen–17 depletion in atmospheric O_2 after a snowball Earth. PNAS 110:14546–14550

Cao X, Liu Y (2011) Equilibrium mass-dependent fractionation relationships for triple oxygen isotopes. Geochim Cosmochim Acta 75:7435–7445

Cappa CD, Hendricks MB, DePalo DJ, Cohen RC (2003) Isotopic fractionation of water during evaporation. J Geophys Res 108(D16):4525

Cernusak LA, Barbour MM, Arndt SK, Cheesman AW, English NB, Field TS, Helliker BR, Holloway-Phillips MM, Holtum JAM, Kahmen A, McInerney FA, Munksgaard NC, Simonin KA, Song X, Stuart-Williams H, West JB, Farquhar GD (2016) Stable isotopes in leaf water of terrestrial plants. Plant Cell Envir 39:1087–1102

Craig H (1961) Isotopic variations in meteoric waters. Science 133:1702–1703

Craig H, Gordon LI (1965) Deuterium and oxygen 18 variations in the ocean and the marine atmosphere. *In* E Tongiorgi, ed. Proceedings of a conference on stable isotopes in oceanographic studies and paleotemperatures, Spoleto, Italy, p 9–130

Criss REC (1999) Principles of stable isotope distribution. Oxford University Press

Dansgaard W (1964) Stable isotopes in precipitation. Tellus 16:436–468

Dennis KJ, Affek HP, Passey BH, Schrag DP, Eiler JM (2011) Defining and absolute reference frame for mass spectrometry. Geochim Cosmochim Acta 75:7117–7131

Ehhalt D, Knott K (1965) Kinetische isotopentrennung bei der verdampfung von wasser. Tellus 17:389–397

Ehleringer JR, Dawson TE (1992) Water-uptake by plants—perspectives from stable isotope composition. Plant Cell Envir 15:1073–1082

Epstein S, Zeiri L (1988) Oxygen and carbon isotopic compositions of gases respired by humans. PNAS 85:1727–1731

Flanagan LB, Comstock JP, Ehleringer JR (1991) Comparison of modeled and observed environmental influences on the stable oxygen and hydrogen isotope composition of leaf water in *Phaseolus vulgaris* L Plant Physiol 96:588–596

Fosu BR, Subba R, Peethambaran R, Ghosh P (2020) Technical note: Developments and applications in triple oxygen isotope analysis of carbonates. ACS Earth Space Chem, in press

Gat JR (1996) Oxygen and hydrogen isotopes in the hydrologic cycle. Annu Rev Earth Planet Sci 24:225–262

Gat JR, Bowser CJ, Kendall C (1994) The contribution of evaporation from the Great Lakes to the continental atmosphere: estimate based on stable isotope data. Geophys Res Lett 21:557–560

Gázquez F, Evans NP, Hodell DA (2017) Precise, accurate fractionation factors ($\alpha^{17}O$, $\alpha^{18}O$, αD) for water and $CaSO_4{\cdot}2H_2O$ (gypsum). Geochim Cosmochim Acta 198:259–270

Gázquez F, Morellón M, Bauska T, Herwartz D, Surma J, Moreno A, Staubwasser M, Valero-Garces B, Delgado-Huertas A, Hodell DA (2018) Triple oxygen and hydrogen isotopes of gypsum hydration water for quantitative paleo-humidity reconstruction. Earth Planet Sci Lett 481:177–188

Gehler A, Tütken T, Pack A (2011) Triple oxygen isotope analysis of bioapatite as a tracer for diagenetic alteration of bones and teeth. Paleaogr Palaeoclim Palaeoecol 310:84–91

Gehler A, Gingerich PD, Pack A (2016) Temperature and atmospheric CO_2 concentration estimates through the PETM using triple oxygen isotope analysis of mammalian bioapatite. PNAS 113:7739–7744

Gibson JJ, Birks SJ, Yi Y (2016) Stable isotope mass balance of lakes: a contemporary perspective. Quat Sci Rev 131B:316–328

Gonfiantini R (1978) Standards for stable isotope measurements in natural compounds. Nature 271:534–536

Guo W, Zhou C (2019a) Triple oxygen isotope fractionation in the DIC–H_2O–CO_2 system: A numerical framework and its implications. Geochim Cosmochim Acta 246:541–564

Guo W, Zhou C (2019b) Patterns and controls of disequilibrium isotope effects in speleothems: Insights from an isotope-enabled diffusion-reaction model and implications for quantitative thermometry. Geochim Cosmochim Acta 267:196–226

Guo W, Mosenfelder JL, Goddard III WA, Eiler JM (2009) Isotopic fractionations associated with phosphoric acid digestion of carbonate minerals: Insights from first-principles theoretical modeling and clumped isotope measurements. Geochim Cosmochim Acta 73:7203–7225

Hayles J, Gao C, Cao X, Liu Y, Bao H (2018) Theoretical calibration of the triple oxygen isotope thermometer. Geochim Cosmochim Acta 235, 237–245

Hofmann MEG, Pack A (2010) Technique for high-precision analysis of triple oxygen isotope ratios in carbon dioxide. Anal Chem 82:4357–4361

Horita J, Rozanski K, Cohen S (2008) Isotope effects in the evaporation of water: a status report of the Craig–Gordon model. Isot Environ Health Stud 44:23–49

Hren MT, Sheldon ND (2012) Temporal variations in lake water temperature: Paleoenvironmental implications of lake carbonate $\delta^{18}O$ and temperature records. Earth Planet Sci Lett 337–338:77–84

Hu H (2016) Triple oxygen isotopes of biominerals: A new proxy for reconstructing paleoaridity, paleoecophysiology, paleo-carbon-cycling. PhD dissertation, Johns Hopkins University (143p)

Jasechko S, Sharp ZD, Gibson JJ, Birks SJ, Yi Y, Fawcett PJ (2013) Terrestrial water fluxes dominated by transpiration. Nature 496:347–350

Ji H (2016) Triple oxygen isotopes in lake waters, lacustrine carbonates, pedogenic carbonates: An indicator for evaporation. PhD dissertation, Johns Hopkins University

Kawagucci S, Tsunogai U, Kudo S, Nakagawa F, Honda H, Aoki S, Nakazawa T, Gamo T (2005) An analytical system for determining $\delta^{17}O$ in CO_2 using continuous flow-isotope ratio MS Anal Chem 77:4509–4514

Kim S-T, Mucci A, Taylor BE (2007) Phosphoric acid fractionation factors for calcite and aragonite between 25 and 75 °C: Revisited. Chem Geol 246:135–146

Koch PL (1998) Isotopic reconstruction of past continental environments. Annu Rev Earth Planet Sci 26:573–613

Kohn MJ (1996) Predicting animal $\delta^{18}O$: Accounting for diet and physiological adaptation. Geochim Cosmochim Acta 60:4811–4829

Kohn MJ, Cerling TE (2002) Stable isotope compositions of biological apatite. Rev Mineral Geochem 48:455–488

Landais A, Barkan E, Yakir D, Luz B (2006) The triple isotopic composition of oxygen in leaf water. Geochim Cosmochim Acta 70:4105–4115

Landais A, Barkan E, Luz B (2008) Record of $\delta^{18}O$ and $\delta^{17}O$-excess in ice from Antarctica during the last 150,000 years. Geophys Res Lett 35:L02709

Landais A, Risi C, Bony S, Vimeux F, Descroix L, Falourd S, Bouygues A (2010) Combined measurement of ^{17}O-excess and d-excess in African monsoon precipitation: Implication for evaluating convective parameterizations. Earth Planet Sci Lett 298:104–112

Landais A, Steen-Larsen HC, Guillevic M, Masson-Delmotte V, Vinther B, Winkler R (2012) Triple isotopic composition of oxygen in surface snow, water vapor at NEEM (Greenland). Geochim Cosmochim Acta 77:304–316

Lehmann SB (2016) Studies of carbon, oxygen,, strontium isotopes in tooth enamel: Evaluating paleoenvironmental change in South Africa and expanding the paleoclimate took kit. PhD dissertation, Johns Hopkins University

Levin NE, Cerling TE, Passey BH, Harris JM, Ehleringer JR (2006) A stable isotope aridity index for terrestrial environments. PNAS 103:11201–11205

Li S, Levin NE, Chesson LA (2015) Continental scale variation in ^{17}O-excess of meteoric waters in the United States. Geochim Cosmochim Acta 164:110–126

Li S, Levin NE, Soderberg K, Dennis KJ, Caylor KK (2017) Triple oxygen isotope composition of leaf waters from Mpala, central Kenya. Earth Planet Sci Lett 468:38–50

Liang M-C, Mahata S, Laskar AH, Theimens MH, Newman S (2017) Oxygen isotope anomaly in tropospheric CO_2 and implications for CO_2 residence time in the atmosphere and gross primary productivity. Sci Report 7:13180

Lin Y, Clayton RN, Huang L, Nakamura N, Lyons JR (2013) Oxygen isotope anomaly observed in water vapor from Alert, Canada and the implication for the stratosphere. PNAS 110:15608–15613

Luz B, Kolodny Y (1985) Oxygen isotope variations in phosphate of biogenic apatites, IV Mammal teeth and bones. Earth Planet Sci Lett 75:29–36

Luz B, Barkan E (2005) The isotopic ratios $^{17}O/^{16}O$ and $^{18}O/^{16}O$ in molecular oxygen and their significance in biogeochemistry. Geochim Cosmochim Acta 69:1099–1110
Luz B, Barkan E (2010) Variations of $^{17}O/^{16}O$ and $^{18}O/^{16}O$ in meteoric waters. Geochim Cosmochim Acta 74:6276–6286
Luz B, Cormie AB, Schwarcz HP (1990) Oxygen isotope variations in phosphate of deer bones. Geochim Cosmochim Acta 54:1723–1728
Luz B, Barkan E, Bender ML, Thiemens MH, Boering KA (1999) Triple-isotope composition of atmospheric oxygen as a tracer of biospheric productivity. Nature 400:547–550
Mahata S, Bhattacharya SK, Wang C-H, Liang M-C (2012) An improved CeO_2 method for high-precision measurements of $^{17}O/^{16}O$ ratios for atmospheric carbon dioxide. Rapid Commun Mass Spectrom 26:1909–1922
Mahata S, Bhattacharya SK, Wang C-H, Liang M-C (2013) Oxygen isotope exchange between O_2 and CO_2 over hot platinum: An innovative technique for measuring $\Delta^{17}O$ in CO_2. Anal Chem 85:6894–6901
Mahata S, Bhattacharya S, Liang MC (2016) An improved method of high-precision determination of $\Delta^{17}O$ of CO_2 by catalyzed exchange with O_2 using hot platinum. Rapid Commun Mass Spectrom 30:119–131
Majoube MF (1971) Fractionnement en oxygène–18 et en deuterium entre l'eau et sa vapeur. J Chem Phys 58:1423–1436
Merlivat L (1978) Molecular diffusivities of $H_2{}^{16}O$, $HD^{16}O$, $H_2{}^{18}O$ in gases. J Chem Phys 69(6):2864–2871
Merlivat L, Jouzel J (1979) Global climatic interpretation of deuterium–oxygen-18 Relationship for precipitation. J Geophys Res 84:5029–5033
Merrit DA, Hayes JM (1994) Factors controlling precision and accuracy in isotope-ratio-monitoring mass spectrometry. Anal Chem 66:2336–2347
Miller MF, Pack A (2021) Why measure ^{17}O? Historical perspective, triple-isotope systematics and selected applications. Rev Mineral Geochem 86:1–34
Miller MF, Franchi IA, Thiemens MH, Jackson TL, Brack A, Kurat G, Pilinger CT (2002) Mass-independent fractionation of oxygen isotopes during thermal decomposition of carbonates. PNAS 99:10988–10993
Mrozek DJ, van der Veen C, Kliphuis M, Kaiser J, Weigel AA, Röckmann T (2015) Continuous-flow IRMS technique for determining the ^{17}O excess of CO_2 using complete oxygen isotope exchange with cerium oxide. Atmos Meas Tech 8:811:822
Nagy KA, Peterson CC (1988) Scaling of water flux rate in animals. University of California Publications in Zoology 120:1–172. University of California Press
New M, Lister D, Hulme M, Makin I (2002) A high-resolution data set of surface climate over global land areas. Clim Res 21:1–25
Pack (2021) Isotopic traces of atmospheric O_2 in rocks, minerals, and melts. Rev Mineral Geochem 86:217–240
Pack A, Herwartz D (2014) The triple oxygen isotope composition of the Earth mantle and understanding $\Delta^{17}O$ variations in terrestrial rocks and minerals. Earth Planet Sci Lett 390:138–145
Pack A, Gehler A, Süssenberger A (2013) Exploring the usability of isotopically anomalous oxygen in bones and teeth as a paleo-CO_2-barometer. Geochim Cosmochim Acta 102:306–317
Pack A, Höweling A, Hezel DC, Stefanak MT, Beck A-K, Peters STM, Sengupta S, Herwartz D, Folco L (2017) Tracing the oxygen isotope composition of the upper Earth's atmosphere using cosmic spherules. Nat Commun 8:15702
Passey BH, Ji H (2019) Triple oxygen isotope signatures of evaporation in lake waters and carbonates: A case study from the western United States. Earth Planet Sci Lett 518:1–12
Passey BH, Hu H, Ji H, Montanari S, Li S, Henkes G, Levin NE (2014) Triple oxygen isotopes in biogenic and sedimentary carbonates. Geochim Cosmochim Acta 141:1–25
Petersen SV,, 29 others (2019). Effects of improved ^{17}O correction on interlaboratory agreement in clumped isotope calibrations, estimates of mineral-specific offsets, and temperature dependence of acid digestion fractionation. Geochem Geophys Geosyst 20:3495–3519
Prasanna K, Bhattacharya SK, Ghosh P, Mahata S, Liang M-C (2016) Isotopic homogenization, scrambling associated with oxygen isotopic exchange on hot platinum: Studies on gas pairs (O_2, CO_2), (CO, CO_2). RSC Adv 6:51296–51303
Prokhorov I, Kluge T, Janssen C (2019) Laser absorption spectroscopy of rare and doubly substituted carbon dioxide isotopologues. Anal Chem 91:15491–15499
Roden JS, Lin G, Ehleringer JR (2000) A mechanistic model for interpreting hydrogen and oxygen isotope ratios in tree-ring cellulose. Geochim Cosmochim Acta 64:21–35
Rowley DB, Garzione CN (2007) Stable isotope-based paleoaltimetry. Annu Rev Earth Planet Sci 35:463–508
Sakai S, Matsuda S, Hikida T, Shimono A, McManus JB, Zahniser M, Nelson D, Dettman DL, Yang D, Ohkouchi N (2017) High-precision simultaneous $^{18}O/^{16}O$, $^{13}C/^{12}C$, and $^{17}O/^{16}O$ analyses for microgram quantities of $CaCO_3$ by tuneable infrared laser absorption spectroscopy. Anal Chem 89:11846–11852
Sha L, Mahata S, Duan P, Luz B, Zhang P, Baker J, Zong B, Ning Y, Ait Brahim Y, Zhang H, Edwards RL, Cheng H (2020) A novel application of triple oxygen isotope ratios of speleothems. Geochim Cosmochim Acta 270:360–378
Sharma T, Clayton RN (1965) Measurement of O^{18}/O^{16} ratios of total oxygen in carbonates. Geochim Cosmochim Acta 29:1347–1353

Sharp ZD, Wostbrock JAG, Pack A (2018) Mass-dependent triple oxygen isotope variations in terrestrial materials. Geochem Perspec Lett 7:27–31

Steig EJ, Gkinis V, Schauer AJ, Shoenemann SW, Samek K, Hoffnagle J, Dennis KJ, Tan SM (2014) Calibrated high-precision ^{17}O-excess measurements using cavity ring-down spectroscopy with laser-current-tuned cavity resonance. Atmos Meas Tech 7:2421

Stewart MK (1975) Stable isotope fractionation due to evaporation and isotopic exchange of falling waterdrops: Applications to atmospheric processes and evaporation of lakes. J Geophys Res 80:1133–1146

Surma J, Assonov S, Bolourchi MJ, Staubwasser M (2015) Triple oxygen isotope signatures in evaporated water bodies from the Sistan Oasis, Iran. Geophys Res Lett 42:8456–8462

Surma J, Assonov S, Herwartz D, Voigt C, Staubwasser M (2018) The evolution of ^{17}O-excess in surface water of the arid environment during recharge and evaporation. Sci Rep 8:4972

Surma J, Assonov S, Staubwasser M (2021) Triple oxygen isotope systematics in the hydrologic cycle. Rev Mineral Geochem 86:401–428

Tian C, Wang L, Kaseke KF, Bird BW (2018) Stable isotope compositions (δ^2H, $\delta^{18}O$, $\delta^{17}O$) of rainfall and snowfall in the central United States. Sci Rep 8:6712

Uechi Y, Uemura R (2019) Dominant influence of the humidity in the moisture source region on the ^{17}O-excess in precipitation on a subtropical island. Earth Planet Sci Lett 513:20–28

Uemura R, Barkan E, Abe O, Luz B (2010) Triple isotope composition of oxygen in atmospheric water vapor. Geophys Res Lett 37:L04402

Voarintsoa NRG, Barkan E, Bergel S, Vieten R, Affek HP (2020) Triple oxygen isotope fractionation between $CaCO_3$ and H_2O in inorganically-precipitated calcite and aragonite. Chem Geol, in press

Wang Z, Nelson DD, Dettman DL, McManus JB, Quade J, Huntington KW, Schauer AJ, Sakai S (2020) Rapid and precise analysis of carbon dioxide clumped isotopic composition by tunable infrared laser differential spectroscopy. Anal Chem 92:2034–2042

White JWC (1989) Stable hydrogen isotope ratios in plants: a review of current theory, some potential applications. *In:* Applications of Stable Isotopes in Ecological Research. PW Rundel, JR Ehleringer, KA Nagy (eds) Springer-Verlag, New York, p 142–160

Whiteman JP, Sharp ZD, Gerson AR, Newsome SD (2019) Relating $\Delta^{17}O$ values of animal body water to exogenous water inputs and metabolism. BioSci 69:658–688

Wostbrock JAG, Cano EJ, Sharp ZD (2020) An internally consistent triple oxygen isotope calibration of standards for silicates, carbonates and air relative to VSMOW2 and SLAP2. Chem Geol 533:119432

Yeung LY, Hayles JA, Hu H, Ash JL, Sun T (2018) Scale distortion from pressure baselines as a source of inaccuracy in triple-isotope measurements. Rapid Commun Mass Spec 32:1811–1821

Young ED, Galy A, Nagahara H (2002) Kinetic and equilibrium mass-dependent fractionation laws in nature and their geochemical and cosmochemical significance. Geochim Cosmochim Acta 66:1095–1104

Young ED, Yeung LY, Kohl IE (2014) On the $\Delta^{17}O$ budget of atmospheric O_2. Geochim Cosmochim Acta 135:102–125